Lysogenic control of Bacillus subtilis morphology and fitness by Spbetavirus phi3T

Floccari V.A.; Feddersen, H.; Jakin Lazar, J.; Grosboillot, V.; Munk, A.; Kempen, P.; ... ; Dragoš, A.

communications biology

A Nature Portfolio journal

Article

https://doi.org/10.1038/s42003-025-08672-x

Lysogenic control of *Bacillus subtilis* morphology and fitness by *Spbetavirus* phi3T

Valentina A. Floccari[1], Helge Feddersen[2], Jaka Jakin Lazar[1], Virginie Grosboillot[1], Anna Munk[3], Paul Kempen[4,5], Robert Hertel[6], Tomaž Accetto[1], Ákos T. Kovács[7], Marc Bramkamp[2] & Anna Dragoš[1]

In lysogenic conversion, temperate phages can profoundly alter the phenotypes of their bacterial hosts. When studying the effects of SPbeta-like viruses on a *Bacillus subtilis* soil isolate, we observed that phage phi3T induced a stable and heritable acquisition of a spherical cell morphology, departing from the typical rod shape of its ancestor. Although time-lapse imaging revealed that the lysogen retained cell wall integrity and symmetric division, it exhibited reduced fitness and increased susceptibility to cell wall-targeting antimicrobials. Remarkably, when SPβ, a homologous SPbeta-like virus, was present, the host retained its rod-shaped morphology despite phi3T superinfection. This study uncovers a novel example of lysogenic conversion in which phage integration into the bacterial genome induces heritable changes in host biology. Additionally, we revealed intriguing phage-phage interactions during polylysogeny that may benefit the host. These findings offer insight into the persistence and absence of specific *Spbetavirus* variants in natural *B. subtilis* populations.

Bacteriophages (or phages) are the most abundant biological entities distributed worldwide[1]. Because they are obligate intracellular parasites, they must infect a bacterial host to replicate, and are classified as virulent or temperate based on their life cycle occurring after infection. Virulent phages can only follow the lytic cycle, hijacking the host's replicative machinery and using lysins to kill the host and to release newly formed phage particles[2]. On the other hand, a temperate phage can follow either lytic or lysogenic cycles, depending mainly on the growth stage and viability of the host. In the lysogenic cycle, the phage infection can be followed by DNA integration into the bacterial chromosome in specific integration sites, through site-specific recombination[3], or random transposition[4], establishing long-term coexistence in the form of a prophage, including replication within the host DNA[2,5]. Under inducing conditions, which vary depending on the specific phage and host, the prophage excises from the host chromosome and enters a lytic cycle[6]. However, there are temperate phages that, upon infection, can be maintained extrachromosomally[7], with genomes can be either circular[8] or linear[9].

Although phage-host interactions are among the most studied antagonistic relationships, the case of temperate phages is particularly complex[10,11]. Owing to long-term coexistence with the host and partly shared reproductive interests, prophages are able to trigger lysogenic conversion by carrying and expressing genes that can strongly influence the physiology of the host[12]. Well-known examples of lysogenic conversion can influence a variety of bacterial traits including production of new metabolic enzymes[13], toxins, and bacteriocins[14], temporal changes and restoration of dormancy[15,16], surface attachment proteins[17], and antiviral defense systems[18].

Certain temperate phages can also modify host phenotypes via specific integration and excision[19]. In the so-called Regulatory Switch (RS) mechanism, the RS phage integrates into a specific host gene whose function is temporarily interrupted, and which can be restored after regulatory excision of the prophage. The best studied examples of RS phages are SPβ and phi3T that belong to genus *Spbetavirus* and target the beneficial bacterium *Bacillus subtilis*. Phage SPβ integrates into the sporulation-specific *spsM* gene, which encodes an enzyme involved in the legionaminic acid biosynthesis pathway[20]. Its integration/excision into this target gene appears to be responsible for phenotypic changes related to spore surface and dispersibility[21], and may potentially influence

[1]Department of Microbiology, Biotechnical Faculty, University of Ljubljana, Ljubljana, 1000, Slovenia. [2]Institute of General Microbiology, Kiel University, Kiel, 24098, Germany. [3]DTU Bioengineering, Technical University of Denmark, Kgs Lyngby, 2800, Denmark. [4]National Center for Nano Fabrication and Characterization, Technical University of Denmark, Kgs Lyngby, Denmark. [5]Department of Health Technology, Technical University of Denmark, Kgs Lyngby, Denmark. [6]Department of Genomic and Applied Microbiology, Georg-August-University of Göttingen, Göttingen, 37077, Germany. [7]Institute of Biology, Leiden University, Leiden, 2333 BE, The Netherlands. e-mail: anna.dragos@bf.uni-lj.si

biofilm formation[22]. Phage phi3T integrates into the *kamA* gene encoding L-lysine 2,3-aminomutase[23,24]. Regulatory excision of both SPβ and phi3T occurs in the spore mother cells, restoring the function of both *spsM* and *kamA* genes prior to sporulation[21,25,26]. Importantly, such mother cell-specific regulatory excision does not lead to lytic cycle induction and formation of virions[26]. In addition, SPβ and phi3T have been well studied recently as they encode anti-defense proteins that overcome the host's infection immunity strategies[27–29].

The lytic cycle of SPβ and phi3T can be triggered by typical DNA-damaging agents such as mitomycin C[16,27,30], allowing horizontal transmission to a new host[14]. It was recently shown that SPβ and phi3T encode arbitrium signaling systems that are involved in phage lysis-lysogeny decision[31]. While SPβ and phi3T are closely related, they use different signal-receptor pairs, and no cross-talk was observed between their arbitrium systems[31–33]. Both SPβ and phi3T are temperate double-stranded DNA (dsDNA) phages characterized by a large genome size of ~130 kbp, and they share 61% homology with each other[16]. SPβ gives the name to the genus, and is also present in the domesticated laboratory strain *B. subtilis* 168[34–36], and in various natural isolates[37]. Unlike SPβ, the phi3T phage has been obtained from an environmental sample via enrichment[38]. Although phi3T lysogens can be easily obtained under laboratory conditions[30,36], phi3T has never been detected as native prophage in *B. subtilis* isolates, even in large-scale ecological studies of *B. subtilis* prophage repertoires[14,37].

In this study, we investigated the consequences of lysogeny by phi3T and SPβ using the natural *B. subtilis* soil isolate P9_B1[39]. This strain is closely related to the laboratory strains *B. subtilis* 168 and NCBI 3610, but it is non-lysogenic for neither SPβ nor phi3T despite being susceptible to both phages. We show that lysogeny for phage phi3T causes a change in P9_B1 host cell morphology from the conventional rod shape to a more spherical shape. We confirm this aberrant phenotype triggered by phi3T in several *B. subtilis* strains, including laboratory strains and natural isolates that otherwise lack SPbeta-like viruses. We also demonstrate consequences of phi3T lysogeny for host competitive fitness and susceptibility to antimicrobials, connecting changes in host cell morphology to possible alterations in cell wall composition. Finally, we discover that lysogeny by SPβ can rescue the *B. subtilis* host from morphology change triggered by phi3T. Our study reveals a novel example of lysogenic conversion in which a phage triggers heritable changes in host cell biology. While host and phage viability are maintained, these host morphology changes are associated with reduced fitness and decreased resistance to cell wall-targeting antimicrobials. Our work also reveals an interesting phage-phage interaction during superinfection, which may benefit the host, possibly explaining the stability and absence of certain SPβ-variants in natural *B. subtilis* populations.

Methods

Strains, media, and culture conditions

Bacterial strains used in this study are listed in Table 1. All lysogenic strains were obtained based on the natural soil isolate *B. subtilis* P9_B1 (NCBI genome accession number: CP045811.1)[39].

Strain *B. subtilis* Δ6 (ΔSPβ Δ*skin* ΔPBSX Δprophage 1 *pks*::cat Δprophage 3), a 168 derivative strain characterized by six large deletions of prophages, was used as an indicator strain in plaque assays and as a host for efficient phage propagation[40]. Lysogenic variants of *B. subtilis* P9_B1 were obtained by cultivating the target strain in lysogeny broth (LB-Lennox; 10 mg mL^{-1} tryptone, 5 mg mL^{-1} yeast extract, 5 mg mL^{-1} NaCl) at 37°C with shaking at 220 rpm, until mid-exponential phase, followed by addition of phage lysate at a multiplicity of infection (MOI) of ~10 and overnight incubation. The next day, strains were streaked onto LB with 1.5% agar medium to obtain single colonies, and colony PCR was performed to confirm prophage integration. Genomic DNA (gDNA) was extracted according to manufacturer protocol with Plant & Fungi DNA Purification Kit (EURx), and integration was confirmed again by PCR. Double lysogens were then obtained. To obtain *B. subtilis* P9_B1 DTUB264, *B. subtilis* P9_B1 DTUB231 was lysogenized with phage phi3T; to obtain *B. subtilis* P9_B1^{SPβ*_phi3T}, *B. subtilis* P9_B1^{SPβ} Δ*spsM* was lysogenized with phage phi3T. The lysogenic strains *B. subtilis* DTUB263, *B. subtilis* DTUB259, *B. subtilis* Δ6^{phi3T}, and *B. subtilis* PY79^{phi3T} were obtained by lysogenizing strains *B. subtilis* 168 ΔSPβ, *B. subtilis* 3610 ΔSPβ, *B. subtilis* Δ6, and *B. subtilis* PY79, respectively, with phage phi3T.

Transformation experiments were performed by adapting the Losick-lab protocol[41] using competence medium prepared fresh from a 10× concentrated stock.

In order to obtain *B. subtilis* strains P9_B1 DivIVA-GFP, P9_B1^{phi3T} DivIVA-GFP, P9_B1 CotB-GFP, and P9_B1^{phi3T} CotB-GFP, gDNA from donor strains *B. subtilis* 1803 and *B. subtilis* JLG 2352 was transformed into *B. subtilis* P9_B1 and P9_B1^{phi3T}, and integrated into the *amyE* locus using selection for respective antibiotic markers (Table 1). The *B. subtilis* P9_B1 MreB-GFP and P9_B1^{phi3T} MreB-GFP strains were obtained by first transforming the gDNA from *B. subtilis* 168 KS36 into *B. subtilis* P9_B1 and P9_B1^{phi3T} (to delete the original *mreB* gene), and selection of the transformants on plates supplemented with antibiotic marker and additionally with 20 mM $MgSO_4$ to rescue the growth of Δ*mreB* strains[42]. Next, the newly obtained *mreB*-null transformants were transformed with gDNA from the donor strain *B. subtilis* KS69 (Table 1), with the MreB-GFP protein fusion construct integrated in *amyE* locus. Transformants were checked for successful integration in the *amyE* locus by PCR using primer pairs *amyF*/*amyR*, and for specific cell morphology by microscopy. Primers used in this study are listed in Table 2.

Strain P9_B1 Δ*kamA* was obtained by transforming gDNA from *B. subtilis* DTUB202 into *B. subtilis* P9_B1. Successful transformation was confirmed by PCR using primer pair oAD36/oAD37, and morphology was examined by microscopy.

Both *B. subtilis* P9_B1^{SPβ_phi3T} GFP and P9_B1^{SPβ_phi3T} mKate were obtained by transforming plasmids phy_sGFP[43] and pTB498[44], respectively, extracted from *Escherichia coli* MC1061 according to manufacturer protocol with QIAprep® Spin Miniprep Kit (Qiagen). The morphology and fluorescence of the transformants were confirmed by microscopy.

The gDNA of five strains from the *B. subtilis* Knockout Erythromycin (BKE; Erm^R) collection (Table 1), each characterized by deletion of one of the target genes *ydaL*, *ydaM*, *ydaN*, *ppsC*, and *ndoA*, were transformed into both P9_B1 and P9_B1^{phi3T} to inactivate the respective genes. The obtained transformants were screened for potential morphology changes using microscopy.

Working concentrations of antibiotics were 5 μg mL^{-1} for kanamycin (Kan) and chloramphenicol (Cm), and 100 μg mL^{-1} for spectinomycin (Spec).

B. subtilis strains were routinely grown in liquid LB medium and shaken at 220 rpm, or on solid medium using LB with 1.5% agar (35 mg mL^{-1}Sigma LB Lennox with agar), at 37°C overnight.

Phage storage, propagation, and counting

All phages used in this study are listed in Table 3. The temperate phages required for the experiments were stored in the lysogenic state within the bacterial host as -80°C glycerol stocks. To obtain phage lysates, the lysogenic strains were grown in baffled shake flasks and induced by adding 0.1 μg mL^{-1} mitomycin C (MMC) in mid-exponential phase to trigger prophage induction, followed by cultivation for another 6 h. In parallel, spontaneous phage induction (SPI) was tested, in which lysogenic strains were allowed to grow without any stress-inducing agent. Cells were pelleted by centrifugation at 8000× g for 10 min at room temperature (RT), discarded, and the supernatant was filter-sterilized (0.2 μm filter) and stored at 4°C. Phage titer and plaque morphology were assessed by double-layered soft-agar (0.3%) assay using *B. subtilis* Δ6 as an indicator strain, followed by plate incubation for 16−20 h at 28°C. Plaques were imaged using an SMZ25 stereomicroscope (Nikon).

To confirm phage identity, single plaques were tested by plaque PCR using specific primer pairs (Table 2). Plaques yielding expected PCR products were carefully removed from the soft agar using a sterile scalpel, resuspended in 300 μL of SM buffer (5.844 mg mL^{-1} NaCl, 1.970 mg mL^{-1} $MgSO_4{\cdot}7H_2O$, 7.880 mg mL^{-1} Tris-HCl, pH 7.5), stored at 4°C, and further

Table 1 | Strains used in this study

Strain name	Genotype	Reference
B. subtilis Δ6	ΔSPβ Δskin ΔPBSX Δprophage 1 pks::cat Δprophage 3, Cm	40
B. subtilis P9_B1	WT	39
B. subtilis P9_B1 DTUB248	Lysogen for phi3T prophage (*kamA*)	This work
B. subtilis P9_B1 DTUB231	Lysogen for SPβ prophage (*spsM*)	14
B. subtilis P9_B1 DTUB264	Lysogen for SPβ (*spsM*) and phi3T (*kamA*) prophages	This work
B. subtilis P9_B1^{SPβ*_phi3T}	Lysogen for SPβ (*yxzL*) and phi3T (*kamA*) prophages	This work
B. subtilis P9_B1^{Goe11}	Lysogen for Goe11 prophage (*kamA*)	This work
B. subtilis P9_B1^{Goe13}	Lysogen for Goe13 prophage (*spsM*)	This work
B. subtilis P9_B1^{Goe14}	Lysogen for Goe14 prophage (*spoVK*)	This work
B. subtilis P9_B1^{SPβ} Δ*spsM*	*amyE*::hy-GFP (CmR) *ypqP*::km, lysogen for SPβ prophage (*yxzL*)	14
B. subtilis 168	Lysogen for SPβ	89,90
B. subtilis NCIB 3610	Lysogen for SPβ	91
B. subtilis 1A747 PY79	Lab strain derived from 168	92
B. subtilis DTUB263	168 SPβ::ery, lysogen for phi3T prophage	This work
B. subtilis DTUB259	3610 SPβ::ery, lysogen for phi3T prophage	This work
B. subtilis PY79^{phi3T}	Lysogen for phi3T prophage	This work
B. subtilis Δ6^{phi3T}	Lysogen for phi3T prophage	This work
B. subtilis 1803	DivIVA-GFP/ *divIVA*::pSG1612 (P*divIVA*-gfp *divIVA* + cat)	51
B. subtilis JLG 2352	*cotB*-GFP-kan	Curtesy of Dr. Javier Lopez Garrido
B. subtilis P9_B1 DivIVA-GFP	DivIVA-GFP/ *divIVA*::pSG1612 (P*divIVA*-gfp *divIVA* + cat)	This work
B. subtilis P9_B1 CotB-GFP	*cotB*-GFP-kan	This work
B. subtilis P9_B1^{phi3T} DivIVA-GFP	DivIVA-GFP/ *divIVA*::pSG1612 (P*divIVA*-gfp *divIVA* + cat), lysogen for phi3T prophage	This work
B. subtilis P9_B1^{phi3T} CotB-GFP	*cotB*-GFP-kan, lysogen for phi3T prophage	This work
B. subtilis 168 KS36	*Ωneo*3427 Δ*mreB* (km)	93
B. subtilis P9_B1 Δ*mreB*	*Ωneo*3427 Δ*mreB* (km)	This work
B. subtilis P9_B1^{phi3T} Δ*mreB*	*Ωneo*3427 Δ*mreB* (km), lysogen for phi3T prophage	This work
B. subtilis KS69	*amyE::spc* Pxyl-*msfgfp-mreB* (spec)	94
B. subtilis P9_B1 MreB-GFP	*amyE::spc* Pxyl-*msfgfp-mreB* (spec)	This work
B. subtilis P9_B1^{phi3T} MreB-GFP	*amyE::spc* Pxyl-*msfgfp-mreB* (spec), lysogen for phi3T prophage	This work
B. subtilis DTUB202	3610 *comI- kamA*::km	16
B. subtilis P9_B1 Δ*kamA*	*kamA*::km	This work
B. subtilis P9_B1 Δ*kamA*^{phi3T}	*kamA*::km, lysogen for phi3T prophage	This work
E. coli MC1061	phy_sGFP, amp (cm)	43
E. coli MC1061 TB 498.1	pTB498, amp (spec)	44
B. subtilis P9_B1 DTUB43	*amyE*::gfp, cm	14
B. subtilis P9_B1 DTUB222	*amyE*::mKate, spec	14
B. subtilis P9_B1 DTUB250	*amyE*::gfp, cm, lysogen for phi3T prophage	This work
B. subtilis P9_B1 DTUB260	*amyE*::mKate, spec, lysogen for phi3T prophage	This work
B. subtilis P9_B1 DTUB235	*amyE*::gfp (cm), lysogen for SPβ prophage	14
B. subtilis P9_B1 DTUB236	*amyE*::mKate (spec), lysogen for SPβ prophage	14
B. subtilis P9_B1^{SPβ_phi3T}	*amyE*::gfp (cm), lysogen for SPβ and phi3T prophages	This work
B. subtilis P9_B1^{SPβ_phi3T}	amyE::mKate (spec), lysogen for SPβ and phi3T prophages	This work
B. subtilis BKE18320	*ppsC*::ery	This work
B. subtilis BKE04300	*ydaM*::ery	This work
B. subtilis BKE0431	*ydaN*::ery	This work
B. subtilis BKE04290	*ydaL*::ery	This work
B. subtilis BKE04660	*ndoA*::ery	This work
B. subtilis P9_B1 Δ*ppsC*	*ppsC*::ery	This work
B. subtilis P9_B1 Δ*ydaM*	*ydaM*::ery	This work
B. subtilis P9_B1 Δ*ydaN*	*ydaN*::ery	This work
B. subtilis P9_B1 Δ*ydaL*	*ydaL*::ery	This work

Table 1 (continued) | Strains used in this study

Strain name	Genotype	Reference
B. subtilis P9_B1 Δ*ndoA*	*ndoA*::ery	This work
B. subtilis P9_B1^{phi3T} Δ*ppsC*	*ppsC*::ery, lysogen for phi3T prophage	This work
B. subtilis P9_B1^{phi3T} Δ*ydaM*	*ydaM*::ery, lysogen for phi3T prophage	This work
B. subtilis P9_B1^{phi3T} Δ*ydaN*	*ydaN*::ery, lysogen for phi3T prophage	This work
B. subtilis P9_B1^{phi3T} Δ*ydaL*	*ydaL*::ery, lysogen for phi3T prophage	This work
B. subtilis P9_B1^{phi3T} Δ*ndoA*	*ndoA*::ery, lysogen for phi3T prophage	This work

propagated to higher titers (at least 10^7 plaque-forming units [PFU] mL^{-1}) using *B. subtilis* Δ6. Prior to lysogenization, lysates were reassessed for titer and uniform plaque morphology.

In the specific case of *B. subtilis* P9_B1 Δ*kamA*, an alternative method was used, because the conventional lysogenization protocol described above was not successful. After phi3T isolation, it was spotted on a LB 0.3% agar plate on a *B. subtilis* P9_B1 Δ*kamA* lawn, where the strain has been plated in exponential phase (OD_{600} ~ 0.4). After 12 h of incubation, only the turbid spots observed have been sampled and streaked on fresh LB kanamycin plates. Afterwards, several colonies have been tested for the presence of phi3T, using primers specific for the phi3T transposase (oAD38/oAD39). Positive clones have been further tested for phage release under both SPI and MMC 0.1 μg mL^{-1} induction conditions.

Growth assay

The growth dynamics of the obtained single and double lysogens were tested and compared with those of the *B. subtilis* P9_B1 WT strain. Overnight cultures of selected lysogens were subjected to measurement of optical density at 600 nm (OD_{600}), pelleted by centrifugation (8000 × *g*, 5 min, RT), and resuspended in 0.9% NaCl to achieve equal starting optical densities. These samples were inoculated at 1% into LB and distributed in 96-well microtiter plates with 200 μL per well. Cultivation was performed using a Cytation 3 Cell Imaging Multi-Mode Reader (Agilent Technologies) at 37°C with linear continuous shaking (3 mm), and OD_{600} was monitored every 10 min for 24 h. Four replicates were included for each strain.

CFU assay

The strains *B. subtilis* P9_B1 WT, P9_B1^{phi3T} and P9_B1^{SPβ} were treated as described in the section "Growth assay". Then, aliquots of 100 μL for each strain were taken from specific wells of the 96-well plate to perform serial dilutions in 0.9% NaCl, and 100 μL of the dilutions of interest were plated on LB 1.5% agar plates. Strains were sampled at five time points (0 – 2 h – 4 h – 6 h – 8 h). Plates were incubated for 12 h and individual colonies were counted. Three biological replicates, and three technical replicates for each biological replicate, were included for each strain.

Competition assay

Overnight cultures of selected, fluorescently-labelled lysogens were subjected to measurement of OD_{600}, pelleted by centrifugation (8000 × *g*, 5 min, RT), and resuspended in 0.9% NaCl to achieve equal starting optical densities (OD_{600} = 5). The WT strain was pre-mixed with a lysogenic strain labeled with a different fluorescent reporter in a 1:1 co-culture. Co-cultures were inoculated at 1% into fresh LB medium and distributed in 96-well microtiter plates with 200 μL per well. Cultivation was performed using a Cytation 3 Cell Imaging Multi-Mode Reader (Agilent Technologies) at 37°C with linear continuous shaking (3 mm), and monitoring the OD_{600}, the green fluorescence channel (excitation/emission 485/528; gain 35) and the red fluorescence channel (excitation/emission 585/635; gain 35) every 10 min for 24 h. Four replicates were included for each strain.

Sporulation assay

Sporulation was performed by inoculating P9_B1 WT and P9_B1^{phi3T} in Casein-Hydrolysate (CH) medium, according to Sterlini & Mandelstam[45], and cultivating cells at 37°C and 220 rpm until OD_{600} reached 0.8. Cells were subsequently centrifuged at 8000× g for 5 min, resuspended in Resuspension Medium[45], and incubated for 16 h at 37°C and 220 rpm. At the end of the incubation period, a fraction of the cells was directly taken to count colony-forming units (CFU). Another fraction was heat-treated at 80°C for 20 min before counting CFU. The percentage of sporulation was calculated as ($CFU_{\text{heat-treated cells}}$ / $CFU_{\text{non-treated cells}}$) × 100.

Spore morphology

Strains were incubated at 37°C with shaking at 220 rpm for 24 h allowing sporulation. The following media were used: new sporulation medium (NSM) (8.00 mg mL^{-1} nutrient broth, 1.00 mg mL^{-1} KCl, 0.2465 mg mL^{-1} $MgSO_4{\cdot}7H_2O$, 0.1641 mg mL^{-1} $Ca(NO_3)_2$, 0.0278 mg mL^{-1} $FeSO_4{\cdot}7H_2O$, 0.0126 mg/mL and mg mL^{-1} $MnCl_2$), LB medium and Minimal salts glycerol glutamate (MSgg) medium[46]. Spores were imaged using Axio Vert A1 (Zeiss), 100x in phase contrast. Spore length and width were manually assessed in Fiji, measuring 100 of spores per each strain and each growth medium.

Light and fluorescence microscopy

The morphology of lysogenic strains was assessed by differential interference contrast (DIC) using an LSM800 equipped AxioObserver Z1 inverted microscope (Zeiss) equipped with a 100× magnification lens (NA 1.4). Strains carrying fluorescent reporter fusion constructs obtained by transformation were examined using the same microscope plus a 488 nm laser to measure green fluorescence with a pinhole size set to 1.0 AU, and a 561 nm laser for red fluorescence with a pinhole size set to 1.2 AU. The Total internal reflection fluorescence (TIRF) imaging of the strains *B. subtilis* P9_B1 MreB-GFP and P9_B1^{phi3T} MreB-GFP was performed using an Elyra 7 inverted widefield microscope (Zeiss), equipped with a 64x magnification lens (NA 0.55) and a 488 nm laser line. The correspondent bright-field (BF) images have been taken using Structured illumination microscopy (SIM). The BF and TIRF micrographs were processed by using Fiji software (version 2.1.0/1.53c).

Time-lapse fluorescence microscopy

B. subtilis reporter fusion construct strains were inoculated from overnight streaked on LB with 1.5% agar and grown in fresh minimal synthetic medium of Davies (MD) (10.7 mg mL^{-1} K_2HPO_4, 6 mg mL^{-1} KH_2PO_4, 1 mg mL^{-1} Na_3 citrate, 20 mg ml^{-1} glucose, 50 μg mL^{-1} L-tryptophan, 11 μg mL^{-1} ferric ammonium citrate, 2.5 mg mL^{-1} L-aspartate pH 7.0, and 0.36 mg mL^{-1} $MgSO_4$, supplemented with 1 mg mL^{-1} casamino acids[47]) at 37°C in baffled shake flasks (220 rpm) to an OD_{600} of 0.5 (exponential phase).

Subsequently, cultures were diluted in fresh MD medium to OD_{600} of 0.035 for monocultures and OD_{600} of 0.07 for cocultures, spotted on pre-warmed (37°C) 1.5% MD agarose pads supplemented with FM4-64 dye (1 mmol L^{-1} final concentration), and incubated for 10 min at 37°C before time-lapse microscopy imaging.

For sporulation assays implying time-lapse microscopy, a different sporulation medium was used (0.98 mg mL^{-1} $FeCl_3{\cdot}6H_2O$, 8.3 mg mL^{-1} $MgCl_2{\cdot}6H_2O$, 19.79 mg mL^{-1} $MnCl_2{\cdot}4H_2O$, 53.5 mg mL^{-1} NH_4Cl, 10.6 mg mL^{-1} Na_2SO_4, 9.7 mg mL^{-1} NH_4NO_3, 50 mg mL^{-1} L-glutamic

Table 2 | Primers used in this study

Primers	Fw/Rev	Target region	Sequence	Description
oAD1	Fw	*sprA*	ATCTGGACTGGCACCTTATGGATACC	+ oAD3: *att*R SPβ
oAD2	Rev	*sprB*	CTGCTCTGGAAAGGAAGGCAGAGTAA	+ oTB122: *att*L SPβ
oAD3	Rev	*ypqP*	ATGACCGAACCTCTGGAACCGAGAAC	+ oAD1: *att*R SPβ + oTB122: intact *spsM* gene
oAD36	Fw	*kamA*	CCGCATTCAGTCTCTTTC	+ oAD37: intact *kamA* gene
oAD37	Rev	*kamA*	GGAAGGAGATCGAGTTATGG	+ oAD36: intact *kamA* gene
oAD38	Fw	phi3T transposase	CTCTGTGGGCATCACTTC	+ oAD39: presence of phi3T
oAD39	Rev	phi3T transposase	CTGGTAGCTCAGCTAAAG	+ oAD38: presence of phi3T
oAD42	Fw	*yokU*	CAGCTGATCCTCAATCTC	+ oAD43: *att*L phi3T
oAD43	Rev	phi3T_end	TTGCACCGTCACATAC	+ oAD42: *att*L phi3T
oAD44	Fw	phi3T_start	CGCCTTTCTTCTCCTG	+ oAD45: *att*R phi3T
oAD45	Rev	*kamA*	GCCGCTTTCTGAAGAAATGC	+ oAD44: *att*R phi3T
oAD61	Fw	*sunT*	GCAACATGTGCCTGCTGAAG	+ oAD62: Sublancin (presence of SPβ)
oAD62	Rev	*sunI*	GGTATGCCATATGCTCAACC	+ oAD61: Sublancin (presence of SPβ)
oTB122	Fw	*phy*	TATTGAGCTTGCCAAACTCATAAGAATGAA	+ oAD2: *att*L SPβ +oAD3: intact *spsM* gene
oVF003	Fw	Prophage gene	TTTGAGAGCGTGTGAGTG	+ oVF004: presence of Goe11, Goe13, Goe14
oVF004	Rev	Prophage gene	CGCTTCCTGAAAGTAGTC	+ oVF003: presence of Goe11, Goe13, Goe14
amyF	Fw	*amyE*	TCTCCAGTGTTCACATCGGTTTG	+ *amyR*: *amyE* locus
amyR	Rev	*amyE*	GCAAGAGAAAAGTTTTGTCTGATTTATG	+ *amyF*: *amyE* locus
oVF005	Fw	*yodQ/yodS*	ACTTGAGCATCCGCATCCTCC	+ oVF006: region between *kamA* and *spsM*
oVF006	Rev	*yodQ/yodS*	CTTGATTGAAGAGGCGCTGAC	+ oVF005: region between *kamA* and *spsM*
oVF007	Fw	*cgeE/cgeC*	GGCGATGGACAGCATTTCTTTC	+oVF008: region between *kamA* and *spsM*
oVF008	Rev	*cgeE/cgeC*	GATTCTGCCGTAACCGTTTCAC	+oVF007: region between *kamA* and *spsM*

Table 3 | List of phage source strains

Strain name	Genotype	Reference
B. subtilis CU1065 1L1	lysogen for phi3T prophage (*kamA*), attSPβ trpC2	30
B. subtilis MB8_B7	WT, lysogen for SPβ prophage (*spsM*)	95
B. subtilis $\Delta6^{Goe11}$	ΔSPβ Δskin ΔPBSX Δprophage 1 pks::cat Δprophage 3, Cm, lysogen for Goe11 prophage	96
B. subtilis $TS01^{Goe13}$	Δ6 derivative, lysogen for Goe13 prophage	96
B. subtilis $TS01^{Goe14}$	Δ6 derivative, lysogen for Goe14 prophage	96

acid, 29.01 mg mL^{-1} $CaCl_2{\cdot}2H_2O$, 245 mg mL^{-1} $MgSO_4{\cdot}7H_2O$, 0.05 mg mL^{-1} L-tryptophan). Briefly, cultures were grown in LB medium at 30°C, 220 rpm overnight for 12 h, diluted in 25% LB to an OD_{600} of 0.1, further cultured at 37°C to OD_{600} of 0.7−0.8, pelleted by centrifugation (4850 rpm, 5 min, 37°C), resuspended in the same volume of sporulation medium, and grown at 37°C. Samples were taken after 3 h and transferred to an agarose pad prepared with 2/3 volume of supernatant from the sporulation culture, 1/3 volume 3.6% agarose in fresh sporulation medium, and 0.5 μg mL^{-1} FM 4-64.

Microscopy images and time-lapse experiments were acquired using an AxioObserver Z1 microscope (Zeiss) equipped with an $OrcaR^2$ camera (Hamamatsu) and a Plan-Apochromat 100× /1.4 oil Ph3 objective (Zeiss). Green fluorescent protein (GFP) fluorescence was visualized with a 38 HE eGFP shift-free filter set (Zeiss) and FM4-64 membrane dye was visualized with a 63 HE mCherry filter set (Zeiss). The microscope was equipped with an environmental chamber set to 37°C. Digital images were acquired with Zen software (Zeiss). Pictures were taken in an environmental chamber at 37°C every 5 min for the phase channel (intensity 60%; exposure time 30 ms), and every 15 min with GFP (λ = 475; intensity 60%; exposure time 100 ms) and mCherry (λ = 555; intensity 50%; exposure time 100 ms) channels, for 16 h in total.

Transmission electron microscopy (TEM)

Bacteria and spores were chemically fixed in a solution of 4% paraformaldehyde and 2% glutaraldehyde in 0.1 M Na cacodylate buffer (pH 7.4). After fixation for 1 h at RT, samples were stored at 4°C until further processing. Samples were rinsed three times in 0.1 M Na cacodylate buffer and pelleted using MiniSpin® plus centrifuge (Eppendorf) at 4000 rpm for 5 min. Cell pellets were suspended in 120 μL of 10% porcine gelatin in 0.1 M Na cacodylate buffer at 37°C for 30 min. Samples were pelleted and placed on ice for 30 min to solidify the gelatin. Excess gelatin was removed and samples were placed in a solution of 1% osmium tetroxide in water at 4°C for 1 h. Samples were rinsed twice in MilliQ water and resuspended in 1% uranyl acetate in water at 4°C overnight. The next morning, samples were rinsed three times in MilliQ water then dehydrated in an increasing ethanol series (50%, 70%, 96%, and 100% for 15 min at each ethanol concentration). Dehydration was carried out at 4°C until the 96% step, after which samples were warmed to RT. Samples were further dehydrated in acetonitrile three times for 5 min each time. Samples were then placed in a 1:1 solution of Embed 812 epoxy resin:acetonitrile for 1 h, followed by a 2:1 solution overnight. The next morning, samples were embedded in pure resin for 1 h before being placed in silicon molds and cured at 60°C overnight. The next day, the cured resin-embedded samples were trimmed with a razor blade

and 100 nm thick sections were cut using a Leica UC7 ultramicrotome equipped with a Diatome diamond knife, and placed on 200 mesh copper TEM grids covered with formvar-reinforced carbon. Samples were imaged using a Tecnai T20 G2 instrument (Thermo Fisher Scientific) operated at 200 kV. Images were acquired using an XF416 CCD camera (TVIPS) and processed using Fiji software.

Genome sequencing, assembly, and verification

The lysogenic strains *B. subtilis* P9_B1 DTUB248 (or P9_B1^{phi3T}), P9_B1 DTUB231 (or P9_B1^{SPβ}), and P9_B1 DTUB264 (or P9_B1^{SPβ_phi3T}, also referred to as double lysogen DL) were sequenced by SeqCenter, LCC (Pittsburgh, PA, USA) by combining Illumina and Nanopore technologies. The lysogenic strain P9_B1 Δ*kamA*^{phi3T} was sequenced by Eurofins Genomics Europe Synthesis GmbH (Germany) by Nanopore technology. Raw sequencing data and assemblies are available from the sequence read archive as follows: P9_B1^{SPβ} (SRX26270955; SRX26270956); P9_B1^{phi3T} (SRX26287360; SRX26287361); P9_B1^{SPβ_phi3T} (SRX26374601; SRX26374600); P9_B1 Δ*kamA*^{phi3T} (SRR34293523). The P9_B1^{SPβ_phi3T} assembly results suggested the presence of both entire prophages as integrated in the respective attachment sites (*att*) in the host chromosome (SPβ in *spsM* and phi3T in *kamA*). To confirm this, P9_B1^{SPβ_phi3T} was tested by genome mapping analysis, performed using both Artemis visualization of Bowtie2 results and CLC software by mapping the Illumina sequencing reads of the DL to the assembled genomes of each lysogen for phi3T and SPβ, to determine the exact contribution of each of the two phages in terms of coverage and percentage of mapping reads. The results indicate an equivalent contribution for each of the two prophages, with 50.686% for phi3T and 49.165% for SPβ, preserving their entire genome length and being integrated separately into the respective integration sites. Finally, the results were further verified by PCR using primer pairs aligning to intact phage *att* genes (oAD3-oTB122 for *spsM*; oAD36-oAD37 for *kamA*), to regions *att*L (oAD2-oTB122 for SPβ; oAD42-AD43 for phi3T) and *att*R (oAD1-oAD3 for SPβ; oAD44-oAD45 for phi3T) to confirm prophages integration, and to chromosomal regions between *att* of both phages (oVF005-oVF006 *yodQ/yodS*; oVF007-oVF008 *cgeE/cgeC*). All alignments, including figures and shared genes information, were obtained using Synphage software (version 0.2.7)[48].

Antimicrobial susceptibility assay

Susceptibility to antimicrobial agents of lysogenic strains *B. subtilis* P9_B1^{phi3T}, P9_B1^{SPβ}, P9_B1^{Goe11}, P9_B1^{Goe13}, and P9_B1^{Goe14} was tested and compared with that of the *B. subtilis* P9_B1 WT strain. Specifically, susceptibility to spectinomycin (Spec), ampicillin (Amp) and D-cycloserine (DCS) was tested. Each experiment was performed testing one antibiotic at a time against the WT strain and one lysogenic strain. OD_{600} values of overnight cultures were measured, cultures were pelleted (8000× g, 5 min, RT), and resuspended in 0.9% NaCl to achieve equal starting optical densities. Cultures were inoculated at 1% in LB and distributed in 96-well microtiter plates with 150 µL per well. Antibiotic was added to inoculated cultures at increasing concentrations from 0 to 200−300 µg mL^{-1} (for Spec, Amp, and DCS). Cultivation was performed using a Cytation 3 Cell Imaging Multi-Mode Reader (Agilent Technologies) at 37°C with linear continuous shaking (3 mm) and monitoring OD_{600} every 10 min for 24 h.

Statistics and reproducibility

Images and movies were edited and analyzed using Fiji software. Analysis involved measuring cell length and width, counting the number of fluorescent cells, and measuring fluorescence intensity. For single cell level measurements, 100 cells within single experimental timepoints were measured using the straight segment line tool. The number of fluorescent cells was counted and fluorescence intensity was measured using the same software mentioned above. Specifically, a greyscale version of the original image was created to enhance the contrast, yielding well-defined individual spores, and the threshold was adjusted to obtain a binary image. To separate individual spores even more effectively, the Watershed operation was employed. After selecting the parameter of interest, and setting a threshold for images and excluding edges, it was finally possible to measure the intensity of individual spores.

For assays performed at the population level (growth, antibiotic susceptibility assay, and competition assay), each strain was cultivated in LB broth with at least four biological replicates, and each experiment was independently repeated at least twice. Statistical differences between experimental groups were then identified using t-test.

No statistical methods were used to predetermine sample size and experiments were not randomized.

Reporting summary

Further information on research design is available in the Nature Portfolio Reporting Summary linked to this article.

Results

Lysogeny by phi3T prophage alters *B. subtilis* cell morphology

While exploring the phenotypic consequences of *Spbetavirus* lysogeny for the *B. subtilis* host, we observed that integration of the phi3T prophage caused a dramatic change in host cell morphology, from a conventional rod to a more spherical shape (Fig. 1a, b). This phenotype mainly manifested in the stationary growth phase, clearly visible after 16 h of incubation in liquid culture or after 4 h of growth on an agarose pad (Fig. 1d, e).

To quantify the differences in cell length and cell width between WT and lysogenic strains, 100 single cells per six selected micrographs were measured using Fiji software from 2 h to 4.5 h of growth, corresponding to early and mid-exponential phases, and additionally after 10 h, corresponding to the stationary phase (Fig. 1f, g). Almost all measurements displayed statistical differences between the two strains ($P < 0.001$; Fig. 1f, g). As expected, the difference in length increased over time, with lysogenic cells significantly shorter than ancestor cells (Fig. 1f). The two strains also displayed differences in width within the exponential phase, when the lysogenic strain was wider, while the two strains had comparable width in the stationary phase (Fig. 1g).

This phenomenon was observed during lysogenization of the natural soil isolate *B. subtilis* P9_B1 (CP045811.1)[39], hereafter referred to as P9_B1 wild type (WT). This strain is a close relative of *B. subtilis* 168[49]. Moreover, the P9_B1 strain, according to our analysis, is not expected to carry any active prophage in its genome (Supplementary Fig. 1). To confirm this, P9_B1 WT and lysogen *B. subtilis* P9_B1^{phi3T} strains were analyzed for spontaneous (SPI) and MMC-triggered prophage induction (Supplementary Fig. 2a). As expected, no plaques were observed for WT, while the lysogen exhibited prophage induction (SPI, 3×10^2 PFU mL^{-1}; MMC, 1.9×10^7 PFU mL^{-1}). Only a single plaque morphology was observed, suggesting that phi3T was the only phage released from P9_B1^{phi3T} (Supplementary Fig. 2a). Both the identity of phi3T and its integration into the host chromosome were confirmed by plaque PCR using specific primers (Supplementary Fig. 2b; see Methods). Afterwards, the entire genome of P9_B1^{phi3T} was sequenced and the integration of the phi3T at the *kamA* locus was further confirmed (Supplementary Fig. 2c; see Methods), as expected according to previous studies focusing on this temperate phage[25].

The prophage phi3T occupies a specific position in the host genome and integrates into the *kamA* gene[19]. Although the gene product was identified as L-lysine 2,3-aminomutase, involvement of the encoded protein in bacterial cell physiology and development is still unknown[30,31]. Therefore, we explored whether there is a link between *kamA* gene disruption and the unconventional spherical phenotype. Cell morphology of the generated *B. subtilis* P9_B1 Δ*kamA* strain was confirmed to be rod-shaped and comparable with WT, excluding the possible involvement of the disrupted *kamA* gene in acquisition of the new peculiar cell morphology phenotype (Fig. 1c). To further confirm that the integration site does not influence the acquisition of the aberrant spherical phenotype upon phi3T phage infection, the *B. subtilis* P9_B1 Δ*kamA* was lysogenized with phi3T prophage. The lysogenization was confirmed by PCR performed on selected lysogen colonies and theirs gDNA (Supplementary Fig. 3a,b; see Methods), and plaque assay

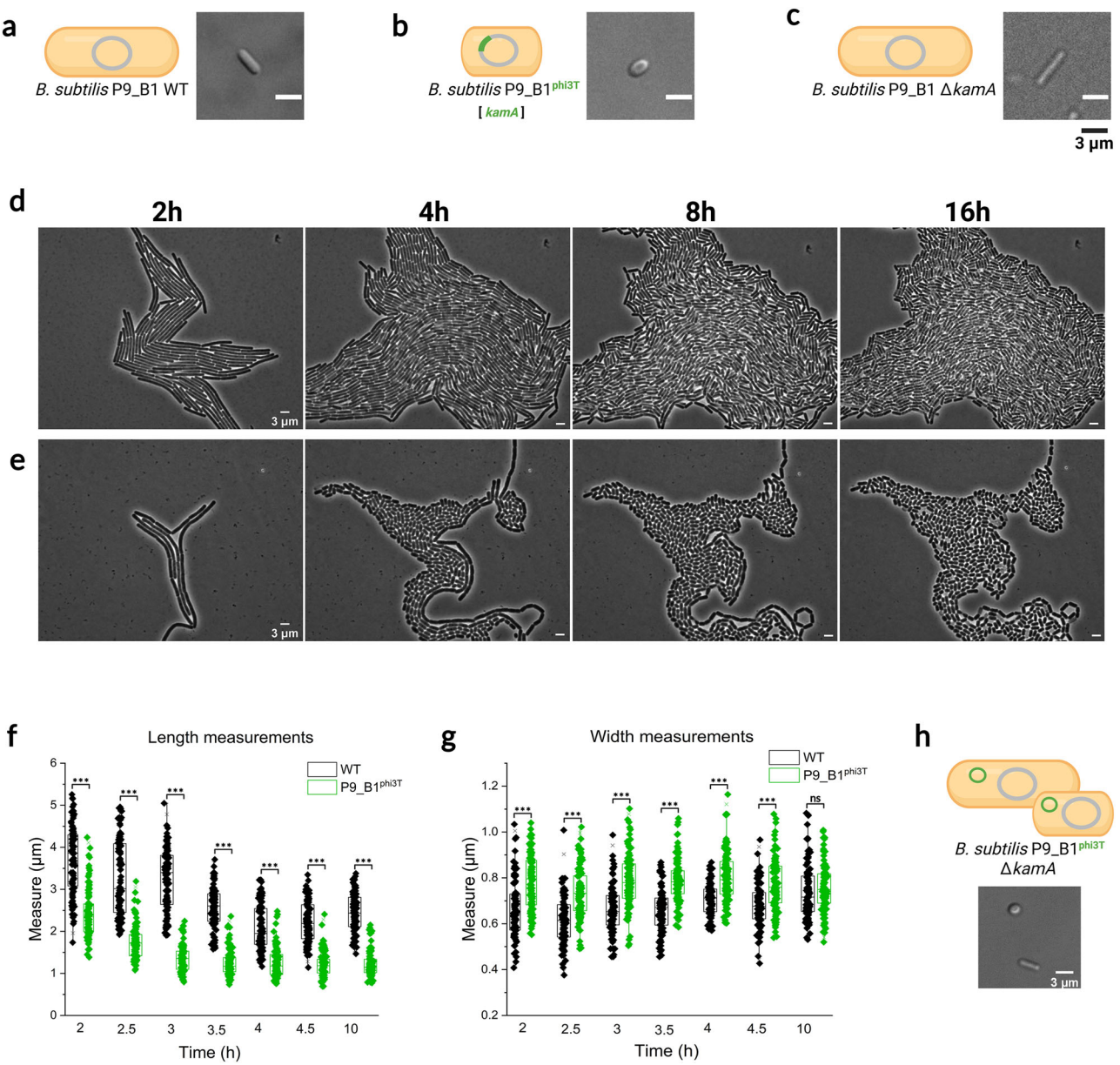

Fig. 1 | Comparison of cell morphology for WT and phi3T lysogen strains. Micrographs and schematic illustrations of (**a**) *B. subtilis* P9_B1 WT, **b***B. subtilis* P9_B1^{phi3T}, and **c** P9_B1 Δ*kamA* strains after 16 h of incubation. Comparison between phase contrast micrographs of monocultures on agarose pad of (**d**) *B. subtilis* P9_B1 WT and (**e**) P9_B1^{phi3T} in terms of growth and division at the same growth stages (after 2, 4, 8 and 16 h). **f** Single cell length and (**g**) width measurements, taken at specific timepoints (from 2 h to 4.5 h of growth, and additionally after 10 h) for both *B. subtilis* P9_B1 WT and P9_B1^{phi3T} strains. Statistical significance is indicated as follows: ns, not significant ($P > 0.05$); *$P < 0.05$; **$P < 0.01$; ***$P < 0.001$. **h** Micrograph depicting cells imaged from *B. subtilis* P9_B1 Δ*kamA*^{phi3T} strain after 16 h of incubation. The schematic representations of bacterial cells were created in BioRender. Floccari, V. A. (2025) https://BioRender.com/vv5oklf.

(Supplementary Fig. 3c). Interestingly, no difference has been observed in terms of PFU mL^{-1} values between the two induction methods (SPI, PFU mL^{-1}: 6 ×109; MMC, PFU mL^{-1}: 7 ×109). Moreover, the microscopy imaging showed the presence of two concomitant morphologies: the conventional rod and the aberrant spherical (Fig. 1h).

The newly obtained lysogen was subjected to Nanopore sequencing. Although the analysis proved the presence of phage phi3T, it did not show that is integrated into the host genome. Indeed, the assembly revealed two separate contigs: contig_0001 (4,063,273 bp) and contig_0002 (128,348 bp). The first was a chromosome of *B. subtilis* P9_B1 Δ*kamA* and the second was a phage phi3T genome.

Together, these results indicate that lysogeny by phi3T alters *B. subtilis* cell shape. This effect is likely due to prophage-encoded protein(s) and seems independent of its stable integration into the host chromosome.

Spherical lysogens possess a cell wall and exhibit no change in cell division or ability to sporulate

As the shape of bacterial cells is generally correlated with the composition of the cell wall according to the scientific literature, the presence and integrity of the cell wall was verified by TEM. In fact, it is known that L-form bacteria, including also *B. subtilis*, can assume an irregular, even spherical morphology due to the complete or partial loss of the cell wall[50]. Therefore, we questioned whether lysogens for the phi3T prophage still have a cell wall, comparable to WT. TEM micrographs of cellular cross-sections showed no evident difference between the cell wall of *B. subtilis* P9_B1 WT (Fig. 2a) and the lysogenic strain (Fig. 2b).

In order to understand the phenomenon underlying the altered cell morphology, the mechanism of cell division was analyzed. We hypothesized that lysogenic cells might divide asymmetrically at certain growth stages.

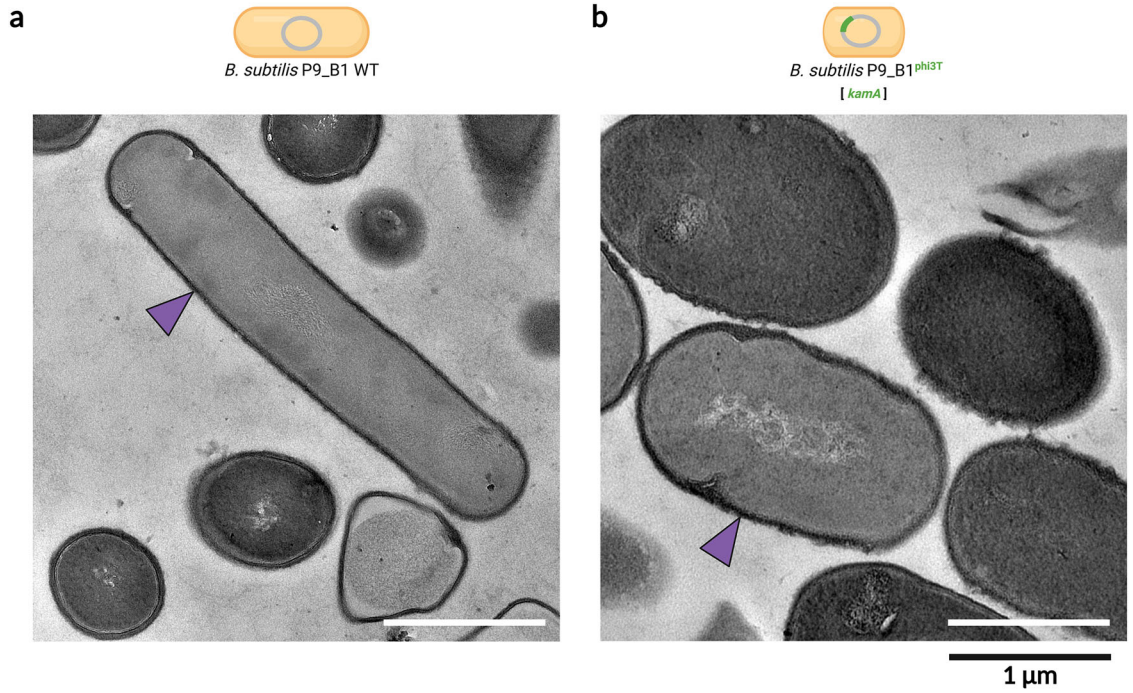

Fig. 2 | Transmission electron micrographs of P9_B1 WT and P9_B1^{phi3T} strains. TEM micrographs depicting sections of vegetative cells of (**a**) *B. subtilis* P9_B1 WT and (**b**) P9_B1^{phi3T}. Purple arrows show the presence of the cell wall in both strains. The schematic representations of bacterial cells were created in BioRender. Floccari, V. A. (2025) https://BioRender.com/b8qfrr1.

First, a time-lapse experiment was performed in which the growth and division of *B. subtilis* P9_B1 WT and P9_B1^{phi3T} was monitored for 16 h (Movie S1 and S2). In contrast to WT cells that maintained the conventional rod shape throughout the experiment (Movie S1), the aberrant spherical phenotype was more pronounced in lysogenic cells after 4 h (in the mid-exponential phase) and was maintained until the stationary phase (Movie S2). Cells of P9_B1^{phi3T} continued to divide even after they started to deviate from rod-shaped morphology. After ~14 h, already in the late stationary phase, some cells of both strains started to lyse, probably due to lack of nutrients and/or limited oxygen (Movie S1 and S2).

The cell membrane intercalating the fluorescent FM4-64 dye was used to localize the position of the division septum. Interestingly, lysogenic cells maintained symmetric division of the mother cell into the two daughter cells, as the septum always localized in the center of the cell (Fig. 3a), as observed for WT cells. This indicates no difference in positioning the septum in the aberrant spherical cells.

Next, we investigated the distribution of the DivIVA protein, a well characterized curvature-sensing protein that acts as a polar scaffold during division and division-site placement. During the exponential phase, DivIVA is flanking the septum at mid-cell, while it is retained at the poles during the stationary phase[51]. Time-lapse experiments with DivIVA-GFP producing *B. subtilis* P9_B1 WT and its phi3T lysogenic version revealed that the DivIVA protein was distributed similarly in the two strains (Fig. 3b). Independently, the correct DivIVA distribution during the stationary phase was also confirmed in single cells grown for 24 h (Fig. 3c).

Thus, the irregular cell shape already manifests in the mid-exponential phase, and it is not likely to be caused by lack of a cell wall, changes in cell division mechanism, or aberrant septum placement.

We also wondered whether the elongation mechanism could be responsible for the acquisition of the spherical shape. In particular, we investigated the possibly different distribution of the actin-like MreB protein, known to play an important role in the determination and maintenance of cell rod shape in bacteria[52,53]. Since MreB is responsible for the localization of the replication machinery, its depletion leads to the loss of the rod phenotype[54]. First, a phenotypic effect of MreB loss was confirmed, as a more spherical morphology was observed in both P9_B1 Δ*mreB* and P9_B1^{phi3T} Δ*mreB* (Supplementary Fig. 4a). Next, the two strains *B. subtilis* P9_B1 and P9_B1^{phi3T} were constructed, both carrying the MreB-GFP protein fusion, and subjected to TIRF imaging at four time points (0 – 2 h – 4 h – 24 h). While P9_B1^{phi3T} MreB-GFP showed constantly a lower fluorescence compared to the WT, no differences have been observed between the two strains in terms of distribution pattern of MreB protein (Supplementary Fig. 4b). Whether the lower fluorescence is related to a lower MreB concentration requires further investigation.

As the lysogenic cells displayed no obvious changes in cell division or elongation regarding MreB, we analyzed their ability to sporulate and germinate (see Methods). Sporulation assays in combination with microscopy analysis clearly indicated the presence of spores (Fig. 3d, e). Specifically, image analysis revealed that >80% of cells sporulated in both strains after 48 h (Supplementary Fig. 5a). Interestingly, spores of P9_B1^{phi3T} showed a shorter and more spherical morphology compared to WT spores (Fig. 3d, e). Moreover, CFU assays confirmed that spores of the lysogen remained viable, as they were able to germinate and form colonies on solid agar medium after heat treatment (Supplementary Fig. 5b; see Methods). Despite the altered spore shape, TEM analysis showed no differences in spore sections. Indeed, spores of both strains exhibited the same amount and distribution of spore layers, consisting of a crust, outer and inner coat, core, and cortex (Supplementary Fig. 5c).

In further support of these results, both strains showed in average similar expression of spore coat protein CotB (Fig. 3f). Interestingly, the fluorescence intensity of the CotB-GFP fusion protein measured at the single cell level displayed more variation among spores of the lysogenic strain, but overall no significant differences between the two strains were detected ($P > 0.05$; Supplementary Fig. 5d). To further confirm that the P9_B1^{phi3T} spores have a different morphology than the P9_B1 WT ones, spores of both strains were grown in three different media (NSM, LB and MSgg) and 100 spores were measured for length and width after imaging. In all three media tested, P9_B1^{phi3T} spores were always shorter than the WT spores ($P < 0.001$). However, the difference in spore width was media

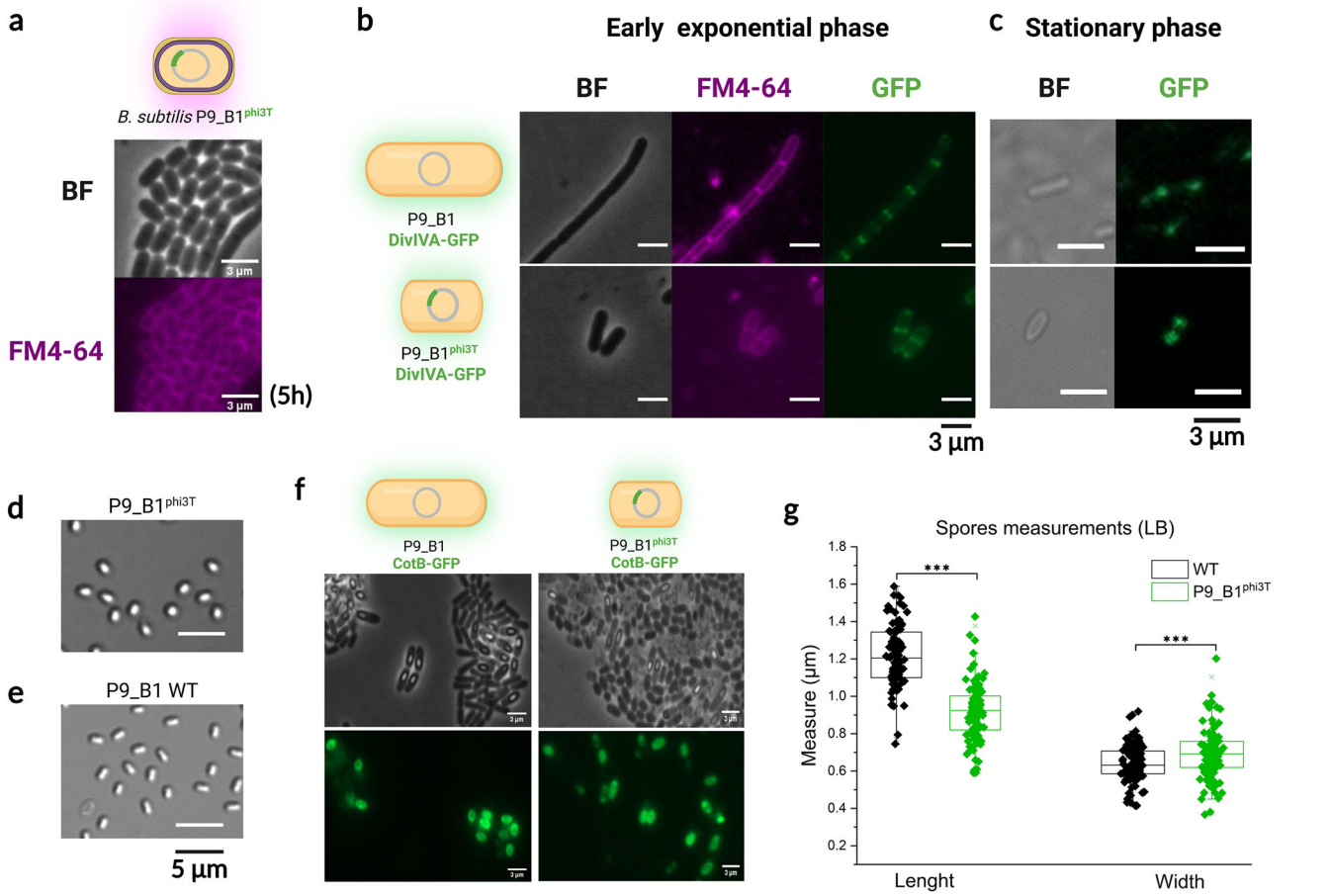

Fig. 3 | Analysis of cell division in WT and phi3T lysogen strains. a Snapshot from time-lapse experiments on *B. subtilis* P9_B1^{phi3T}, showing growing cells stained with FM4-64 after incubation for 5 h. Division septa are visible at mid-cell. **b** Snapshots from time-lapse experiments tracking the distribution of DivIVA-GFP protein in *B. subtilis* P9_B1 DivIVA-GFP and P9_B1^{phi3T} DivIVA-GFP in the early exponential phase. In both strains, the reporter fusion construct is localized in the center of dividing cells. **c** Single cells imaged after 24 h of incubation, showing DivIVA-GFP protein distribution at the poles in the stationary phase. Micrographs of spores of (**d**) *B. subtilis* P9_B1^{phi3T} and (**e**) P9_B1 WT, showing that the lysogenic strain exhibits a peculiar morphology also in the spore state. **f** Snapshots from time-lapse experiments showing comparable CotB-GFP protein expression in the two strains. **g** Length and width measurements of *B. subtilis* P9_B1 WT and P9_B1^{phi3T} spores obtained by growing both strains in LB medium. The statistical significance is indicated as follows: ns, not significant ($P > 0.05$); *$P < 0.05$; **$P < 0.01$; ***$P < 0.001$. The schematic representations of bacterial cells were created in BioRender. Floccari, V. A. (2025) https://BioRender.com/jcfihl3.

dependent, as spores of the lysogen were significantly wider compared to WT spores in LB medium only ($P < 0.001$). (Fig. 3g, Supplementary Fig. 5e).

Lysogeny by phi3T impairs host competitive fitness

Next, the effect of phi3T prophage lysogeny was explored on host fitness. In the presence of the phi3T prophage, a peculiar growth curve was observed, exhibiting differences already in the early exponential phase (Fig. 4a). Overall, the maximum optical density (OD_{max}) was significantly higher for WT cells (Supplementary Fig. 6a). Interestingly, the lysogen exhibited a slightly faster growth rate and doubling time than WT in the early exponential phase (Supplementary Fig. 7a; Supplementary Fig. 6b), but this difference in growth rate was dramatically reverted in the late exponential phase (Supplementary Fig. 7a; Supplementary Fig. 6c), when the lysogen displayed much slower growth than WT. In line with OD measurements, the phi3T lysogen also showed lower CFU values at initial stages of growth (Fig. 4b). A lysogen for SPβ prophage (P9_B1^{SPβ}, DTUB231), a close relative of phi3T phage, was used as an additional control. The significantly lower P9_B1^{phi3T} CFU ml^{-1} relative to the WT and SPβ lysogen were observed after 8 h, a timepoint which coincided with the acquisition of spherical morphology by the lysogen (Fig. 4a–c).

Next, we labeled the strains with constitutive fluorescent reporters (GFP and mKate) and performed a competition assay between P9_B1 WT and P9_B1^{phi3T} in liquid medium, starting from a 1:1 mixed co-culture. The experiments were repeated with the fluorescent reporter swapped. Regardless of the fluorescent marker used, the lysogen for phi3T was consistently at a disadvantage (Fig. 4d; Supplementary Fig. 8). As an additional control, we also included an experiment with the P9_B1^{SPβ} strain, which as expected according to previous results[14], showed a positive effect on host fitness (Supplementary Fig. 9). Overall, the altered cell shape of P9_B1^{phi3T} was accompanied by a lower growth rate, lower maximum yield, and impaired competitive fitness.

Lysogeny by phi3T increases susceptibility to cell wall-targeting antimicrobials

Possible differences in cell wall between the P9_B1 WT strain and the phi3T lysogen were further investigated by testing their susceptibility to cell wall-targeting antibiotics. In particular, two antimicrobial agents were selected that inhibit different cell wall synthesis steps, namely ampicillin (Amp) and D-cycloserine (DCS). Indeed, while ampicillin exerts its inhibition effect in the final steps[55,56] of the cell wall synthesis, D-cycloserine[57] has an effect in the early stages.

For possible differences in antimicrobial susceptibility, the minimum inhibitory concentration (MIC) was determined and compared.

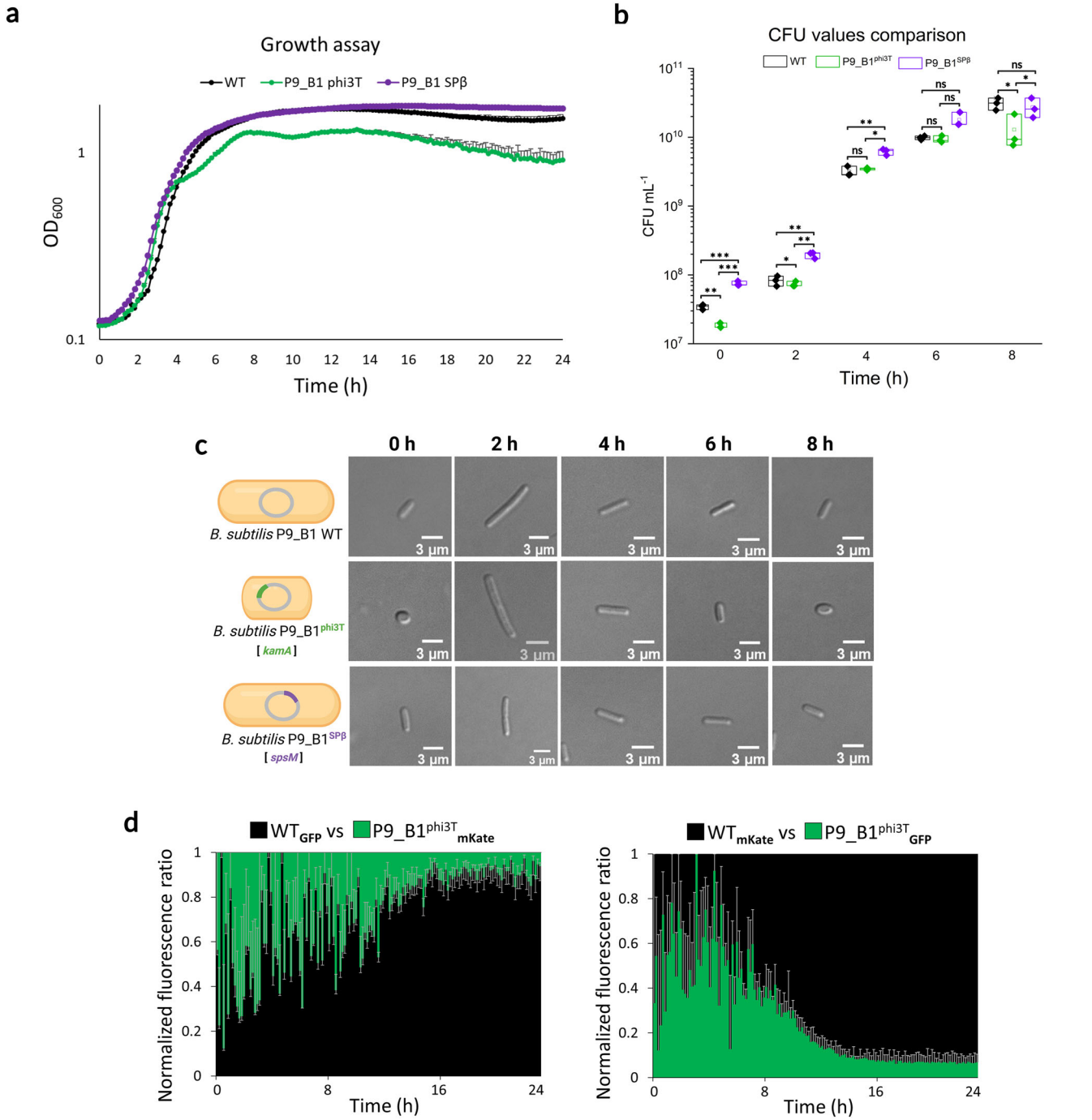

Fig. 4 | Growth dynamics of WT and phi3T lysogen strains, and competition between them. a Growth assay results showing differences in growth dynamics among *B. subtilis* P9_B1 WT (in black), P9_B1^{phi3T} (in green) and P9_B1^{SPβ} (in purple). Only top error bars are shown for each growth curve. **b** Comparison of CFU mL^{-1} values at five time points (0 – 2 h – 4 h – 6 h – 8 h) between the three strains analyzed. The statistical significance is indicated as follows: ns, not significant ($P > 0.05$); *$P < 0.05$; **$P < 0.01$; ***$P < 0.001$. **c** Micrographs showing the single cells from the three strains sampled at the five time points mentioned above. It can be clearly seen how the morphology of P9_B1^{phi3T} changes according to the growth stage, while both WT and P9_B1^{SPβ} retain rod cell morphology and differ only in cell length. **d** Competition assay results in liquid medium. The antagonistic strains were labeled in co-cultures with two different fluorescent proteins (GFP and mKate) and tested in both combinations of fluorescent markers. The schematic representations of bacterial cells were created in BioRender. Floccari, V. A. (2025) https://BioRender.com/xaugkj0.

In all experiments performed, the WT strain always had a higher MIC (Amp, 150 µg mL^{-1}; DCS, 250 µg mL^{-1}) than the P9_B1^{phi3T} strain (Amp, 12 µg mL^{-1}; DCS, 150 µg mL^{-1}; Fig. 5a–c; Supplementary Fig. 10a, b). Additionally, we tested the ampicillin response of P9_B1 DL in comparison with P9_B1 WT, where both strains exhibited the same MIC result (Supplementary Fig. 11). To further connect the lower MIC to potential differences in the host cell wall, we tested the antibiotic spectinomycin (Spec), which has a cytosolic target not related to the cell wall. Interestingly, both WT and phi3T lysogen exhibited similar MICs (50 µg mL^{-1}; Fig. 5c; Supplementary Fig. 12).

Moreover, the hypothesis that the lower MIC registered for phi3T lysogen compared to WT might be linked to possible prophage induction

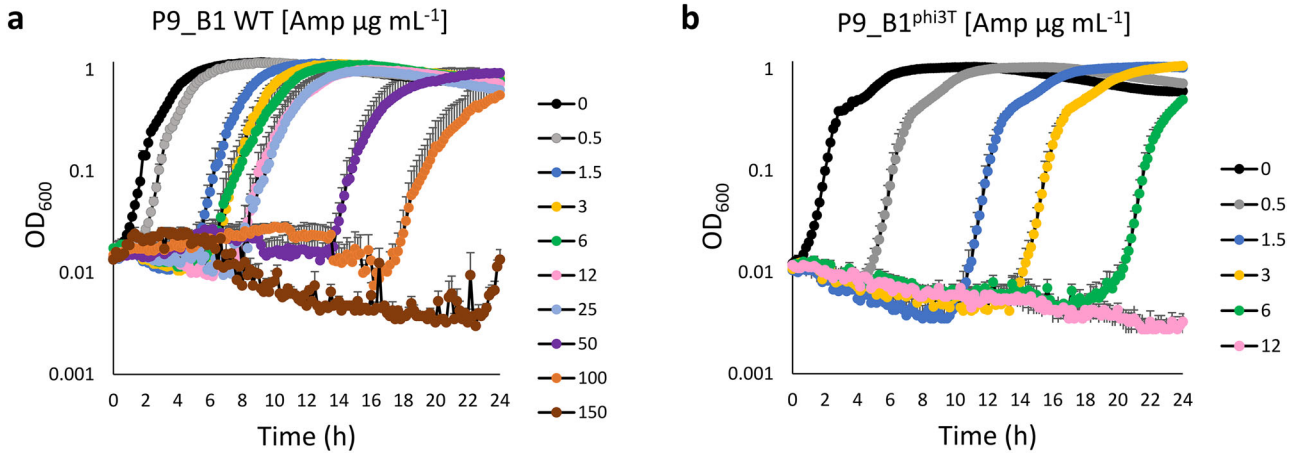

c

Strain name	Amp MIC (µg/mL)	DCS MIC (µg/mL)	Spec MIC (µg/mL)
B. subtilis P9_B1 WT	150	250	50
B. subtilis P9_B1^{phi3T}	12	150	50
B. subtilis P9_B1$^{SP\beta}$	100	250	50
B. subtilis P9_B1^{Goe11}	25	200	50
B. subtilis P9_B1^{Goe13}	100	200	50
B. subtilis P9_B1^{Goe14}	50	200	50
B. subtilis P9_B1 Δ*kamA*	150	/	/

Fig. 5 | Antimicrobial susceptibility assay. a*B. subtilis* P9_B1 WT and **b***B. subtilis* P9_B1^{phi3T} were tested for susceptibility to ampicillin (Amp). For each growth curve, only the top error bars are shown. **c** Table summarizing the results obtained from the antimicrobial susceptibility test, showing MIC values observed for each strain tested, depending on the specific antimicrobial ampicillin (Amp), D-cycloserine (DCS) and spectinomycin (Spec). Differences in susceptibility for each strain are represented as a color code from the darkest (identical to WT) to the brightest (extremely different to the WT).

was rejected by the plaque assay result. In fact, the PFU mL^{-1} value at the MIC of any of the antibiotics tested was not significantly higher than the control (0 µg mL^{-1}) (Supplementary Fig. 13).

Additional SPbeta-like viruses also alter host susceptibility to cell wall-targeting antimicrobials

Next, we investigated whether other phages of the genus *Spbetavirus* could trigger similar changes in cell shape or antibiotic susceptibility during lysogeny of *B. subtilis* P9_B1. The bacterial model strain P9_B1 was lysogenized with three more SPbeta-like viruses, each integrated in a specific integration site in the host chromosome: Goe11 (*kamA*), Goe13 (*spsM*), and Goe14 (*spoVK*). The obtained lysogens, including P9_B1$^{SP\beta}$ (with SPβ integrated into *spsM* gene), were confirmed by PCR and checked for potential morphology changes using single-cell microscopy imaging (Fig. 6a).

Interestingly, the other lysogens showed a conventional rod-shaped morphology (Fig. 6a). Notably, even though phage Goe11 integrates in the same *attB* site as phi3T, it does not lead to any change in host morphology, which further confirms that disruption of the *kamA* gene is not responsible for the aberrant phenotype. Subsequently, all new lysogenic strains were screened for spontaneous (SPI) and MMC-triggered prophage induction. While phage SPβ always displayed the lowest titer (SPI, 2×10^2 PFU mL^{-1}; MMC, 6×10^5 PFU mL^{-1}), increasing only after MMC induction, phage Goe13 always exhibited the highest titer (SPI, 3×10^2 PFU mL^{-1}; MMC, 1.3×10^{11} PFU mL^{-1}), followed by Goe11 (SPI, 6×10^2 PFU mL^{-1}; MMC, 2.4×10^8 PFU mL^{-1}) and Goe14 (SPI, 2×10^2 PFU mL^{-1}; MMC, 1×10^6 PFU mL^{-1}; Supplementary Fig. 14a). Thus, no correlation was observed between the high rate of SPI or MMC-triggered prophage induction and the effect on host cell morphology. Additionally, single plaque morphology varied slightly for each tested lysogen (Supplementary Fig. 14b). While P9_B1^{Goe14} had a slightly shorter lag phase than other lysogens, no dramatic differences in growth dynamics of lysogens were observed compared with WT (Supplementary Fig. 15a,b,c and d).

Next, we compared the responses of other lysogens to cell wall-targeting antibiotics and to spectinomycin. For ampicillin and D-cycloserine, a lower MIC compared to WT was also observed for most of the other lysogens tested, namely P9_B1$^{SP\beta}$ (Amp, 100 µg mL^{-1}; DCS, 250 µg mL^{-1}), P9_B1^{Goe11} (Amp, 25 µg mL^{-1}; DCS, 200 µg mL^{-1}), P9_B1^{Goe13} (Amp, 100 µg mL^{-1}; DCS, 200 µg mL^{-1}), and P9_B1^{Goe14} (Amp, 50 µg mL^{-1}; DCS, 200 µg mL^{-1}; Fig. 5c; Supplementary Fig. 10a,b), while MIC measured for phi3T lysogen was still the lowest. Interestingly, the lowest MIC values were registered only with ampicillin for P9_B1^{phi3T}, P9_B1^{Goe11}, and P9_B1^{Goe14}, two of which possess the *kamA* gene as the *attB* site for the prophage. Since the function of *kamA* has not been described, we explored its possible involvement in the acquisition of a lower MIC by testing the P9_B1 Δ*kamA* strain. The MIC (150 µg mL^{-1}) obtained for the Δ*kamA* strain was identical to that of WT (Fig. 5c; Supplementary Fig. 10a). Similar to the phi3T lysogen, other lysogens did not differ from WT in their susceptibility to spectinomycin (Supplementary Fig. 12). They also did not show an increase in SPI upon exposure to antibiotics (Supplementary Fig. 13).

Finally, we used Synphage software[48] to search for proteins and genes that were shared solely between phi3T, Goe14, and Goe11, that showed the greatest decrease in MIC for cell wall-targeting antibiotics (Fig. 6b). Two genes common to phi3T, Goe14 and Goe11, but absent in SPβ and Goe13 were found: phi3T_2, encoding a putative acetyltransferase, and phi3T_182, encoding a hypothetical protein (Supplementary Table 1). Notably,

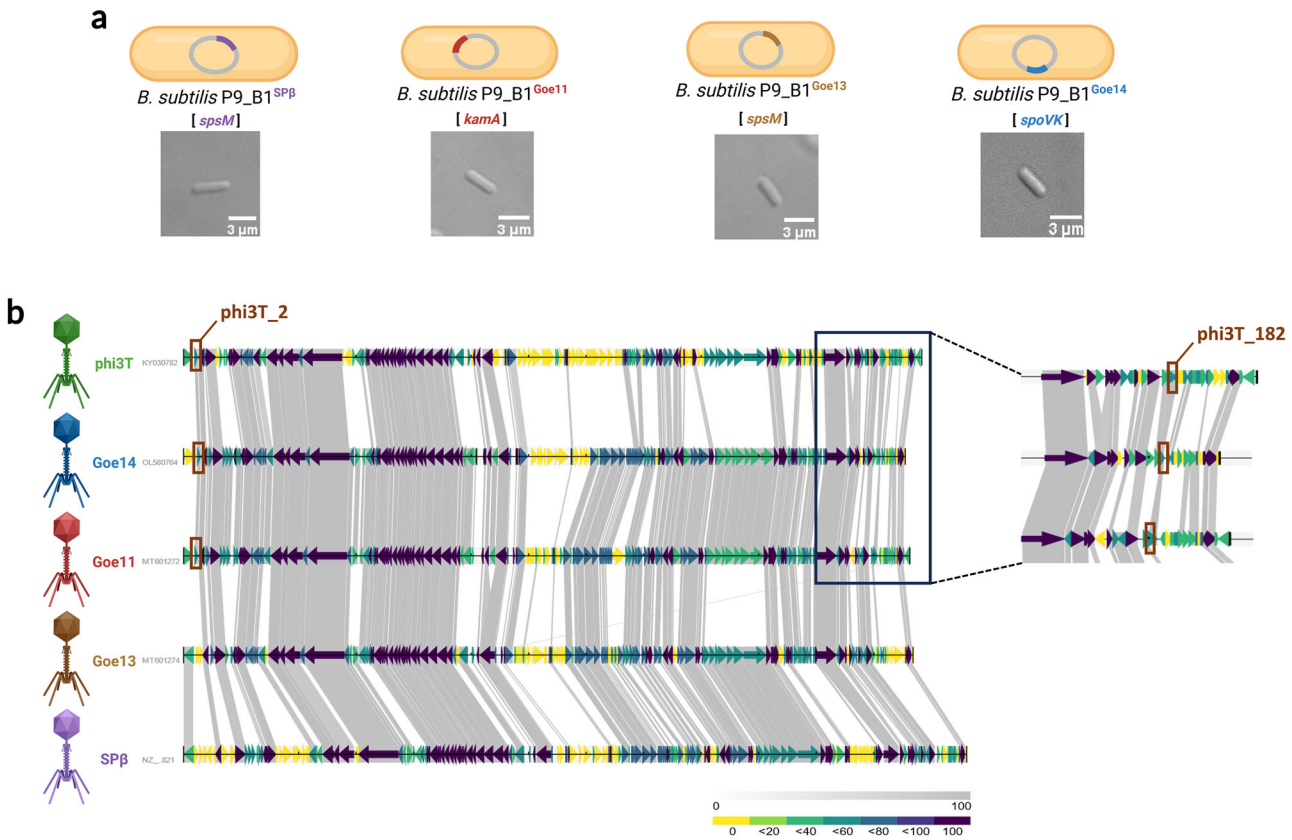

Fig. 6 | Morphologies of strains lysogenized with different SPbeta-like viruses, and phage genome maps. a From left to right, micrographs of single cells taken after 16 h of incubation for strains *B. subtilis* P9_B1^{SPβ}, P9_B1^{Goe11}, P9_B1^{Goe13}, and P9_B1^{Goe14} which show a rod-shaped cell morphology. **b** Genome comparison among all SPbeta-like viruses used in this study, in order from the top to the bottom: phi3T (128 kbp), Goe14 (125 kbp), Goe11 (126 kbp), Goe13 (126 kbp) and SPβ (136 kbp).The genes shared exclusively by phi3T, Goe11, and Goe14 (phi3T_2 and phi3T_182), which may be linked to reduced host ampicillin resistance in the respective *B. subtilis* P9_B1 lysogens compared to the WT strain, are highlighted in brown. The schematic representations of bacterial cells and phage particles were created in BioRender. Floccari, V. A. (2025) https://BioRender.com/vuvl0h0.

presence of the O-acetyltransferase was reported to cause an extensive reduction in penicillin resistance in *Streptococcus pneumoniae*[58]. This suggest that these prophages may encode a protein/component capable of modifying the peptidoglycan of their host, making it more vulnerable to β-lactam and/or other antimicrobials targeting the cell wall. Further experiments are needed to confirm the presence and expression of a similar protein in the abovementioned lysogens.

The Synphage software was additionally used to identify unique features in phi3T phage, revealing a total of 63 genes and 44 proteins (Supplementary Table 2). We hypothesize that the component responsible for the morphological change by phi3T is present within this non-conserved part of the genome.

The effect of phi3T on cell shape is host-specific

While phi3T lysogeny has been explored previously by other researchers[30,31], no change in cell shape was reported. Therefore, we further investigated if the observed spherical phenotype of the P9_B1 lysogen is host strain-specific. We lysogenized a set of different *B. subtilis* hosts, including 168, 3610, Δ6, and PY79, followed by examination of host morphology. Cell morphology became more spherical in *B. subtilis* Δ6^{phi3T}, but the classic rod shape morphology was preserved in 168^{phi3T}, 3610^{phi3T}, and PY79^{phi3T} strains (Fig. 7a). While *B. subtilis* 168 and 3610 strains carry the SPβ prophage in their genome and their "resistance" to phi3T-mediated cell shape change could be due to phage-phage interaction, the PY79 strain is not lysogenic for SPβ.

To understand the lack of comparable responses by PY79 to phi3T lysogeny as observed for P9_B1, we compared their respective genomes (Supplementary Fig. 16a). We identified 21 genes present in *B. subtilis* P9_B1 but absent in PY79, for most of which it was possible to identify the locus in the bacterial genome, but not the predicted function. Three genes (*ydaL*, *ydaM*, and *ydaN*)[59] were selected for further investigation (Supplementary Fig. 16b; Supplementary Table 3), revealing that they are not responsible of the differences between the two aforementioned strains. Additionally, we tested and excluded the possible influence of the two genes *ppsC* (plipastatin synthetase operon)[60,61] and *ndoA* (EndoAI/EndoA toxin/antitoxin system)[62,63] in acquisition of the spherical cell morphology by phi3T.

The presence of SPβ rescues *B. subtilis* from cell morphology changes triggered by phi3T

The presence of SPβ prophage is the major difference between *B. subtilis* 168 and P9_B1. Therefore, we hypothesized that SPβ prevents the phi3T lysogeny-mediated shift in cell shape in the 168 strain. To test this hypothesis, SPβ was first deleted from both *B. subtilis* 168 and 3610 strains. Subsequently, the derived strains were lysogenized with phage phi3T. Both 168 ΔSPβ^{phi3T} and 3610 ΔSPβ^{phi3T} exhibited a spherical morphology (Fig. 7a), just like P9_B1^{phi3T}. Additionally, phi3T was also introduced into P9_B1 pre-lysogenized by SPβ, obtaining the double lysogen (DL) P9_B1^{SPβ_phi3T}. Integration of both phages at their specific loci (*spsM* for SPβ and *kamA* for phi3T) was confirmed by specific primers targeting marginal regions of both prophages and host chromosomes, as well as host regions between *kamA* and *spsM* (Supplementary Fig. 17). However, intact *attB sites* were also amplified, suggesting that excision or spontaneous induction of prophages may occur in subpopulations of cells, as previously described[16]. The presence of both prophages in DL was additionally confirmed by whole-genome sequencing (see Methods).

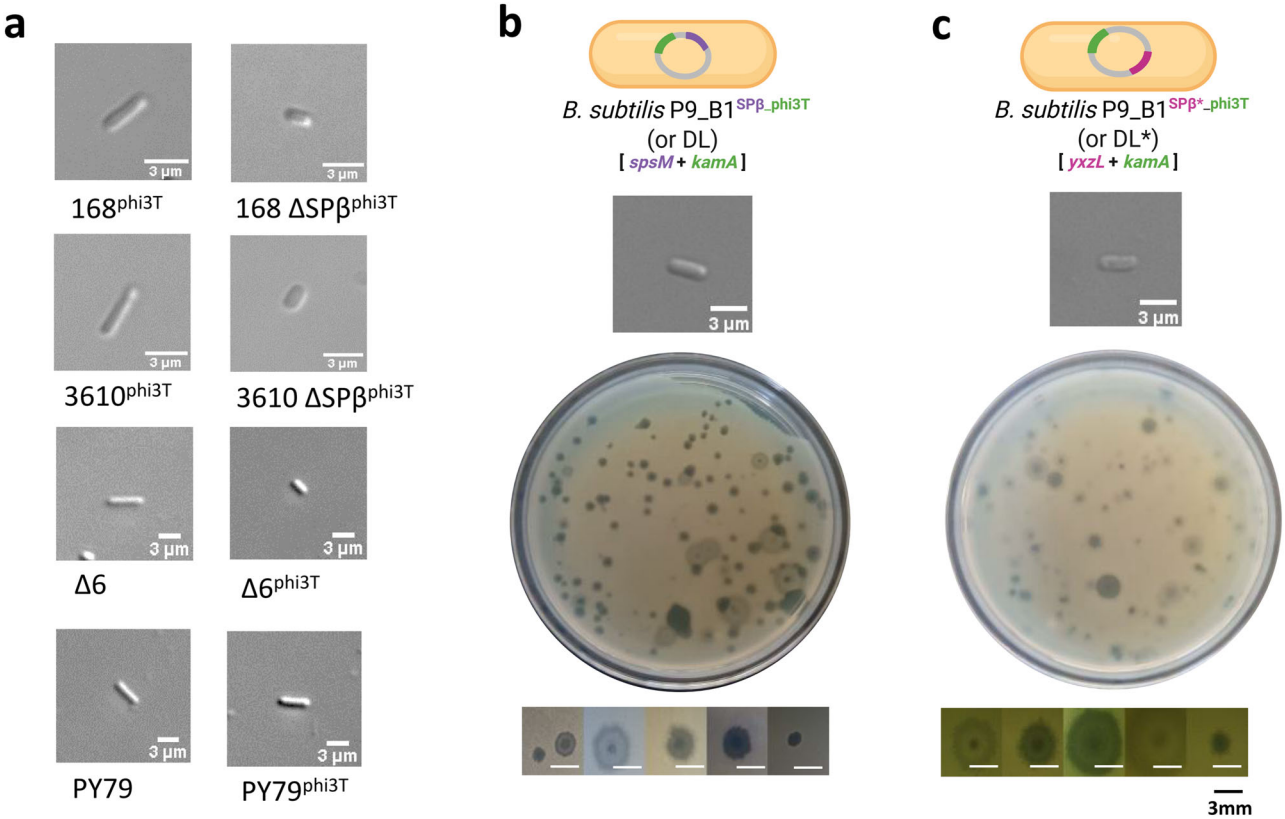

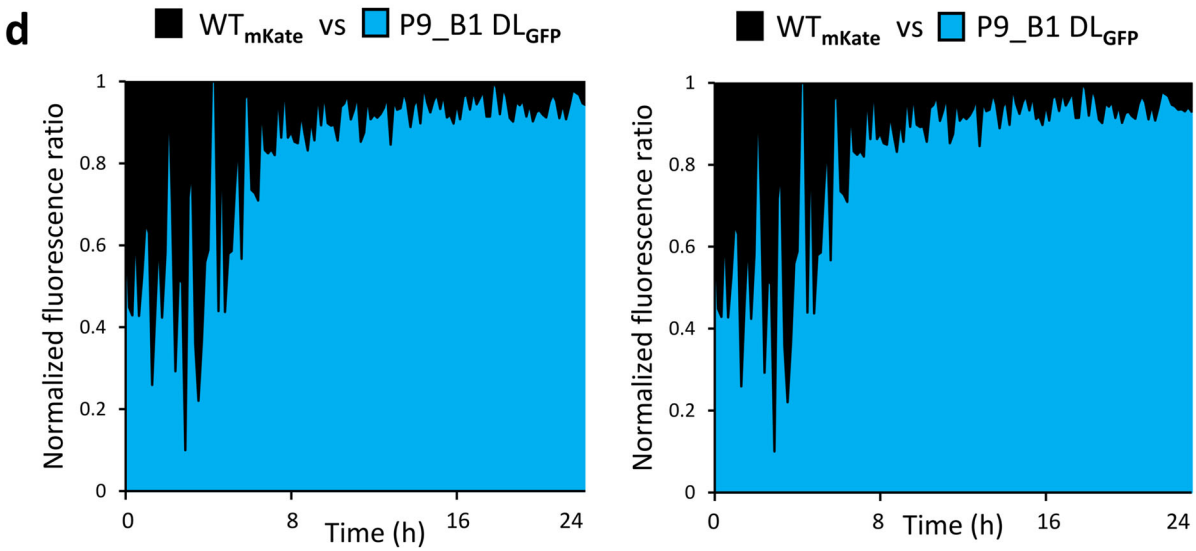

Fig. 7 | Effect of host genetic background and polylysogeny on cell morphology effects caused by phi3T. a From top to bottom, micrographs of single cells showing how phi3T prophage influences the cell morphology of strains *B. subtilis* 168, 3610, and Δ6 when it is the only active prophage in their chromosome. Conversely, phage phi3T seems to have no effect on PY79 cell shape. Micrographs of (**b**) *B. subtilis* P9_B1 DL (lysogen for SPβ and phi3T prophages, respectively integrated in *spsM* and *kamA* host genes) and (**c**) *B. subtilis* P9_B1 DL* (lysogen for SPβ and phi3T prophages, respectively integrated in *yxzL* and *kamA* host genes) single cells taken after 16 h of incubation, showing a rod-shaped cell morphology. Confluent plaque assay results testing *B. subtilis* P9_B1 DL (**b**) and DL* (**c**) lysates on *B. subtilis* Δ6 lawn are also shown. The micrographs show the variety of phage plaques observed in plaque assays. **d** Results of competition assay in liquid medium. The antagonistic strains P9_B1 WT (black) and P9_B1 DL (light blue) were labeled in co-cultures with two different fluorescent proteins (GFP and mKate) to distinguish between them. The schematic representations of bacterial cells were created in BioRender. Floccari, V. A. (2025) https://BioRender.com/qmq9lb7.

As expected, DL maintained the rod-shaped morphology (Fig. 7b). Moreover, a similar lack of cell morphology change compared to the traditional rod cell shape was also observed for the P9_B1$^{SP\beta^*_phi3T}$ (DL*) strain, where SPβ was inserted at the *yxzL* gene[14], distant from phi3T (Fig. 7c). Together, these results strongly suggest that the presence of SPβ rescues *B. subtilis* from cell morphology changes triggered by phi3T.

Finally, we examined the DL and DL* strains for both spontaneous and MMC-triggered prophage induction, followed by plaque assay. Interestingly, a high phage titer was detected from both DL (SPI, 6×10^5 PFU mL^{-1};

MMC, 2.3×10^7 PFU mL^{-1}) and DL* (SPI, 3×10^3 PFU mL^{-1}; MMC, 3×10^6 PFU mL^{-1}) phage supernatants, linked to a variety of plaque morphologies (Fig. 7b, c). There are many reasons underlying the differences in phage plaque size and morphology such as bacterial host, cultivation medium, nutritional state, type of phage, phage genome content, phage absorption rate, and time of lysis[16]. The variable plaque morphologies are likely the result of prophage induction of a superinfected host, and might be explained by the formation of SPβ and phi3T chimeric variants, that display a higher rate of spontaneous induction[16,64].

Lastly, we explored whether the morphology rescue effect in the double lysogens is also associated with fitness rescue. We observed that the DL strain showed a comparable growth dynamic to WT (Supplementary Fig. 15e). Importantly, in contrast to what was observed for WT vs. P9_B1^{SPβ} (where P9_B1^{SPβ} was consistently superior), or WT vs. P9_B1^{phi3T} (where P9_B1^{phi3T} was consistently inferior), the outcome for the DL strain in competition against WT was less obvious (Fig. 7d), even though the fluorescently labeled DL strains behaved as expected, when tested in monocultures (Supplementary Fig. 18). In fact, the simultaneous presence of two prophages and the constitutive expression of a reporter gene could stress the host and affect the outcome of competition. Growth dynamics were also explored by comparing DL* and WT strains, showing a peculiar growth curve for the double lysogen that diverges from WT already in the early exponential phase (Supplementary Fig. 15f).

Since the unconventional spherical phenotype was not observed in the two double lysogens, SPβ may exert a protective role in preventing the morphological shift and negative fitness effects caused by the sole presence of phi3T.

Discussion

Lysogenic conversion[12] resulting from temperate phage-host interaction has been mostly studied in the context of bacterial virulence[65,66], but the specific case of host morphology alteration with preserved viability by an active prophage remains poorly characterized. In this study, we identified an unconventional cell morphology phenotype caused by a phage infection, in which integration of the prophage phi3T caused *B. subtilis* cells to adopt a more spherical shape, while maintaining the ability to divide, sporulate, and germinate.

Bacterial cell shape is determined and maintained by the peptidoglycan cell wall, the first physical barrier to the extracellular environment[67,68]. There are known examples of bacteria whose morphology changes from rod-shaped to a different shape, including spherical, after losing their cell wall[50,69]. Such morphology changes can occur without affecting their viability. This is the case with L-form bacteria, variants that have been naturally or artificially deprived of their cell wall, but are still able to grow and proliferate[50,70]. This cell wall-deficient form allows the acquisition of a different phenotype than the conventional rod-shaped that eventually reverts to the normal (N)-form[50,69]. This phenomenon has also been described for *B. subtilis* under certain laboratory conditions[71].

However, in this work the cell wall was still present in the phi3T lysogen, and no visible differences could be detected between WT and lysogen cells or their spore envelopes. Nevertheless, experiments with antibiotics targeting cell wall synthesis strongly suggest that WT and phi3T lysogen may differ in cell wall composition. Ampicillin and D-cycloserine antibiotics were tested, all of which affect different stages of cell wall peptidoglycan biosynthesis. Ampicillin is a β-lactam antibiotic that exerts its bactericidal effect by interrupting bacterial cell wall biosynthesis as a result of covalent binding to penicillin-binding proteins (PBPs), crucial enzymes involved in the final steps of peptidoglycan cross-linking. As peptidoglycan maintains the integrity of the cell wall, its disruption leads to cell death by lysis[55,56].

D-cycloserine inhibits an early stage of cell wall biosynthesis. It specifically targets enzymes of sequential peptidoglycan biosynthesis, namely alanine racemase (Alr) and D-alanine-D-alanine ligase (D-Ala-D-Ala), by binding to them and irreversibly blocking their catalytic activity[57].

Interestingly, all tested lysogens showed a lower MIC for ampicillin and D-cycloserine, except for P9_B1^{SPβ}, compared with WT, but the phi3T lysogen always had the lowest MIC. The most dramatic effects were observed for ampicillin, suggesting these prophages might specifically interact directly or indirectly with molecules crucial in the late stage of cell wall biosynthesis.

The results of these experiments support the hypothesis that the cell wall of lysogenic strains differs from that of the WT strain. Indeed, a decrease in MIC was observed when lysogens were exposed to antibiotics specifically targeting the cell wall, using the WT strain as a reference. This phenomenon was not observed in the presence of an antibiotic with a cytosolic target, such us spectinomycin. Specifically, this antibiotic inhibits protein synthesis by binding to the 30S ribosomal subunit and blocking initiation of the peptide chain[72,73]. Furthermore, we ruled out that this was related to prophage induction because no increase in PFU was observed in association with increasing antibiotic concentration, suggesting that the presence of phages in the prophage state is sufficient to achieve a lower MIC. We hypothesize that the changes in cell wall composition occur as a result of prophage-encoded components, such as cell wall hydrolases. In particular, virolysins such as holins and endolysins are crucial for bacterial lysis at the end of the lytic cycle[74,75]. Holins are small hydrophobic proteins localized in the inner cell membrane of the bacterial host that assemble into homodimers and form holes[76]. This facilitates access of phage-endolysins to the cell wall, where their selective substrates are located[77]. A specific analysis using techniques such as high-performance liquid chromatography–mass spectrometry (HPLC-MS) and nuclear magnetic resonance (NMR) to characterize the cell wall composition of lysogens would shed light on the possible differences due to the influence of prophages on the bacterial host cell wall. In addition, targeted cloning in P9_B1 WT of unique phage genomic fragments could help to identify the gene/s involved in this phenomenon.

The presence of the prophage may also stimulate the activity of bacterial-encoded lysozymes and/or autolysins[74], or even alter regulation of bacterial hydrolysis involved in remodeling the bacterial cell wall during its biosynthesis[78]. Indeed, it has already been shown that prophages can encode genes that directly/indirectly modulate the expression of host genes and thus influence the physiology of the host[79]. Moreover, modifications in the cell wall could be part of the superinfection exclusion (SIE) mechanism, in which temperate phages can lead to bacterial host modifications to avoid the possibility that other phages may infect the same cell. Supporting this hypothesis, *E. coli* phages maintain cell wall integrity by inhibiting cell wall degradation promoted by other phages[80]. Further work is needed to test the susceptibility of the phi3T lysogen to lytic phages and closely related SPbeta-like viruses.

The phenomenon of altered cell shape was first observed during phi3T lysogeny of the natural soil isolate *B. subtilis* P9_B1[39], which originally carries no active prophages. Interestingly, phi3T does not trigger similar changes in laboratory strain PY79, which was used as a lysogen for phage phi3T in a previous study[81,82]. Moreover, we excluded the involvement of specific integration in *kamA attB* site for the acquisition of the spherical morphology, by observing the same phenomenon occurring also in a mutant deprived of the aforementioned integration site upon phi3T infection. It is possible that the phi3T integrase has a very specific affinity for the *kamA* gene and that if the bacterial strain lacks this gene, phi3T could be maintained as free DNA in the host cytoplasm, probably in an episomal state. This would explain why both morphologies were observed, but also the unusually high spontaneous prophage induction rate.

Surprisingly, phi3T altered the cell shape of the 168-derivative Δ6 strain that lacks prophage elements including SPβ, as well as *B. subtilis* 168 ΔSPβ and NCBI 3610 ΔSPβ. This suggests that phage SPβ plays a protective role in preventing the alteration of cell morphology mediated by phage phi3T. This observation, combined with previously reported beneficial effects of SPβ[14], could explain the prevalence of this Spbeta-like virus within the *B. subtilis* genomes[16]. Recently, however, it has been described that phi3T may have an advantage over SPβ in infections with bacterial hosts

carrying the conjugative element ICE*Bs1*. Indeed, the newly discovered counter-defense gene *nip*, which is carried by phi3T but absent in SPβ, is crucial to prevent the abortive defense mechanism by the ICE*Bs1*-encoded SpbK enzyme[83].

While a similar, stable effect on host morphology triggered by an active prophage has never been reported, a significant change in host cell shape was observed in *Escherichia coli* K-12, which is lysogenic for the cryptic prophage Rac, in response to oxidative stress[84]. Bacterial survival is ensured by KilR, a toxic phage protein that acts as a dual morphogenetic inhibitor of the cell division and cell elongation pathways by interacting, respectively, with the proteins FtsZ and MreBCD[85,86]. Depending on which of the two pathways is affected, the rescued cells acquire either a filamentous or a more lemon-shaped morphology[86]. However, concerning active viruses there are known cases in which viral infection triggers changes in host morphology with harmful consequences for the host. Examples include the phage SPO1, responsible for defective growth and the acquisition of a filamentous morphology in *B. subtilis*. SPO1 phage expresses the Gp46 protein, a histone-like protein (HU) inhibitor that prevents nucleoid segregation[87]. Another remarkable example is the archaeal lemon-shaped virus STSV2, which is responsible for cell gigantism and turns its host into a giant virion factory by interfering with its cell cycle[88]. However, in the aforementioned cases, cell morphology alterations are epigenetic and transient, since they are directly linked to the phage lytic cycle, and followed by host cell death[87,88]. By contrast, the phenotype triggered by phi3T is heritable and stable for at least several generations, and under laboratory growth conditions. Competition assays clearly showed a consistent disadvantage of the lysogen in the presence of the WT strain, which may explain why phi3T has not been detected as a prophage within the genomes of natural *B. subtilis* isolates[16].

Overall, the results of our study show how strongly SPbeta-like viruses influence host physiology in terms of growth dynamics, fitness, and morphology. Moreover, this is the first reported case in which host cell morphology is shaped by lysogenic conversion without affecting bacterial viability. The reason for the acquisition of the aberrant spherical shape following phi3T infection remains an open question, as does the protective function of SPβ during double lysogeny. Further investigation of these unexplored mechanisms could contribute to a better understanding of phage-host interactions, phage-phage interactions occurring during superinfection of the same bacterial host, and the interplay between bacterial pathogens and their RS phages.

Data availability

All relevant data supporting the findings of this study are available within the manuscript and its supplementary information files. Raw sequencing data have been deposited at Sequence Read Archive (SRA) under BioProject PRJNA1172641 and all raw datasets have been deposited at Zenodo https://doi.org/10.5281/zenodo.15771751. Additional datasets generated and analyzed during the current study are available from the corresponding author upon reasonable request.

Received: 24 January 2025; Accepted: 5 August 2025;
Published online: 18 August 2025

References

1. Sharp, R. Bacteriophages: Biology and history. *J. Chem. Technol. Biotechnol.* **76**, 667–672 (2001).
2. Salmond, G. P. C. & Fineran, P. C. A century of the phage: Past, present and future. *Nat. Rev. Microbiol.* **13**, 777–786 (2015).
3. Casjens, S. R. & Hendrix, R. W. Bacteriophage lambda: early pioneer and still relevant. *Virology* **479–480**, 310–330 (2015).
4. Harshey, R. M. Transposable phage Mu. In *Mobile DNA III* (eds. Chandler, M., Gellert, M., Lambowitz, A. M., Rice, P. A. & Sandmeyer, S. B.) 669–691 (ASM Press, 2015).
5. Young, R. Phage lysis: Do we have the hole story yet?. *Curr. Opin. Microbiol.* **16**, 790–797 (2013).
6. Paul, J. H. Prophages in marine bacteria: Dangerous molecular time bombs or the key to survival in the seas?. *ISME J.* **2**, 579–589 (2008).
7. Howard-Varona, C., Hargreaves, K. R., Abedon, S. T. & Sullivan, M. B. Lysogeny in nature: mechanisms, impact and ecology of temperate phages. *ISME J.* **11**, 1511–1520 (2017).
8. Łobocka, M. B. et al. Genome of bacteriophage P1. *J. Bacteriol.* **186**, 7032–7068 (2004).
9. Ravin, N. V. N15: the linear phage-plasmid. *Plasmid* **65**, 102–109 (2011).
10. Floccari, V. A. & Dragoš, A. Host control by SPβ phage regulatory switch as potential manipulation strategy. *Curr. Opin. Microbiol.* **71**, 102260 (2023).
11. Harrison, E. & Brockhurst, M. A. Ecological and evolutionary benefits of temperate phage: What does or doesn't kill you makes you stronger. *BioEssays* **39**, 1700112 (2017).
12. King, R. C., Stansfield, W. D. & Mulligan, P. K. *A Dictionary of Genetics*. (Oxford University Press, 2006).
13. Rohwer, F. & Thurber, R. V. Viruses manipulate the marine environment. *Nature* **459**, 207–212 (2009).
14. Dragoš, A. et al. Phages carry interbacterial weapons encoded by biosynthetic gene clusters. *Curr. Biol.* **31**, 3479–3489 (2021).
15. Kinney, D. M. & Bramucci, M. G. Analysis of *Bacillus subtilis* sporulation with spore-converting bacteriophage PMB12. *J. Bacteriol.* **145**, 1281–1285 (1981).
16. Dragoš, A. et al. Pervasive prophage recombination occurs during evolution of spore-forming *Bacilli*. *ISME J.* **15**, 1344–1358 (2021).
17. Vaca Pacheco, S., Garcıća González, O. & Paniagua Contreras, G. L. The *lom* gene of bacteriophage λ is involved in *Escherichia coli* K12 adhesion to human buccal epithelial cells. *FEMS Microbiol. Lett.* **156**, 129–132 (2006).
18. Rousset, F. et al. Phages and their satellites encode hotspots of antiviral systems. *Cell host microbe* **30**, 740–753 (2022).
19. Feiner, R. et al. A new perspective on lysogeny: Prophages as active regulatory switches of bacteria. *Nat. Rev. Microbiol.* **13**, 641–650 (2015).
20. Dubois, T. et al. The *sps* genes encode an original legionaminic acid pathway required for crust assembly in *Bacillus subtilis*. *MBio* **11**, 1–17 (2020).
21. Abe, K. et al. Developmentally-Regulated Excision of the SPβ Prophage Reconstitutes a Gene Required for Spore Envelope Maturation in Bacillus subtilis. *PLoS Genet* **10**, e1004636 (2014).
22. Sanchez-Vizuete, P. et al. Identification of *ypqP* as a new *Bacillus subtilis* biofilm determinant that mediates the protection of *Staphylococcus aureus* against antimicrobial agents in mixed-species communities. *Appl. I Environ. Microbiol.* **81**, 109–118 (2015).
23. Chen, D., Ruzicka, F. J. & Frey, P. A. A Novel lysine 2,3-aminomutase encoded by the *yodO* gene of *Bacillus subtilis:* Characterization and the observation of organic radical intermediates. *Biochem. J.* **348**, 539–549 (2000).
24. Feucht, A., Evans, L. & Errington, J. Identification of sporulation genes by genome-wide analysis of the σE regulon of *Bacillus subtilis*. *Microbiology* **149**, 3023–3034 (2003).
25. Suzuki, S. et al. Compatibility of site-specific recombination units between mobile genetic elements. *iScience* **23**, (2020).
26. Abe, K., Takamatsu, T. & Sato, T. Mechanism of bacterial gene rearrangement: SprA-catalyzed precise DNA recombination and its directionality control by SprB ensure the gene rearrangement and stable expression of *spsM* during sporulation in *Bacillus subtilis*. *Nucleic Acids Res* **45**, 6669–6683 (2017).
27. Yirmiya, E. et al. Phages overcome bacterial immunity via diverse anti-defence proteins. *Nature* **625**, 352–359 (2024).
28. Zhang, H. et al. Structural insights into activation mechanisms on NADase of the bacterial DSR2 anti-phage defense system. *Sci. Adv.* **10**, eadn5691 (2024).

29. Garb, J. et al. Multiple phage resistance systems inhibit infection via SIR2-dependent NAD^+ depletion. *Nat. Microbiol.* **7**, 1849–1856 (2022).
30. Dou, C. et al. Structural and functional insights into the regulation of the lysis–lysogeny decision in viral communities. *Nat. Microbiol.* **3**, 1285–1294 (2018).
31. Erez, Z. et al. Communication between viruses guides lysis-lysogeny decisions. *Nature* **541**, 488–493 (2017).
32. Gallego del Sol, F., Quiles-Puchalt, N., Brady, A., Penadés, J. R. & Marina, A. Insights into the mechanism of action of the arbitrium communication system in SPbeta phages. *Nat. Commun.* **13**, 3627 (2022).
33. Gallego del Sol, F., Penadés, J. R. & Marina, A. Deciphering the molecular mechanism underpinning phage arbitrium communication systems. *Mol. Cell.* **74**, 59–72 (2019).
34. Zahler, S. A. et al. *Bacillus subtilis* bacteriophage SPbeta: localization of the prophage attachment site, and specialized transduction. *J. Bacteriol.* **129**, 556–558 (1977).
35. Warner, F. D. et al. Characterization of SPβ: a temperate bacteriophage from *Bacillus subtilis* 168M. *Can. J. Microbiol.* **23**, 45–51 (1977).
36. Kohm, K. & Hertel, R. The life cycle of SPβ and related phages. *Arch. Virol.* **166**, 2119–2130 (2021).
37. Stefanič, P. et al. Ecology of prophage-like elements in *Bacillus subtilis* at global and local geographical scales. *Cell Rep*. **44**, (2025).
38. Tucker, R. G. Acquisition of thymidylate synthetase activity by a thymine-requiring mutant of *Bacillus subtilis* following infection by the temperate phage φ3. *J. Gen. Virol.* **4**, 489–504 (1969).
39. Kiesewalter, H. T. et al. Complete genome sequences of 13 *Bacillus subtilis* soil isolates for studying secondary metabolite diversity. *Microbiol. Resour. Announc.* **9**, 10–1128 (2020).
40. Westers, H. et al. Genome engineering reveals large dispensable regions in *Bacillus subtilis*. *Mol. Biol. Evol.* **20**, 2076–2090 (2003).
41. iGEM *B. subtilis* transformation: Losick protocol. https://2013.igem.org/Team:Groningen/protocols/Transformation (2013).
42. Formstone, A. & Errington, J. A magnesium-dependent mreB null mutant: implications for the role of mreB in *Bacillus subtilis*. *Mol. Microbiol.* **55**, 1646–1657 (2005).
43. Van Gestel, J., Weissing, F. J., Kuipers, O. P. & Kovács, ÁT. Density of founder cells affects spatial pattern formation and cooperation in *Bacillus subtilis* biofilms. *ISME J.* **8**, 2069–2079 (2014).
44. Mhatre, E. et al. Presence of calcium lowers the expansion of *Bacillus subtilis* colony biofilms. *Microorganisms* **5**, 7 (2017).
45. Sterlini, J. M. & Mandelstam, J. Commitment to sporulation in *Bacillus subtilis* and its relationship to development of actinomycin resistance. *Biochem. J.* **113**, 29–37 (1969).
46. Branda, S. S., González-Pastor, J. E., Ben-Yehuda, S., Losick, R. & Kolter, R. Fruiting body formation by *Bacillus subtilis*. *Proc. Natl Acad. Sci. USA* **96**, 7311–7316 (1999).
47. Feddersen, H. & Bramkamp, M. Mechanistic insights into MinD regulation and pattern formation in *Bacillus subtilis. eLife* **13**, RP101517 (2024).
48. Grosboillot, V. & Dragoš, A. Synphage: a pipeline for phage genome synteny graphics focused on gene conservation. *Bioinform. Adv.* **4**, vbae126 (2024).
49. Steinke, K., Mohite, O. S., Weber, T. & Kovács, ÁT. Phylogenetic distribution of secondary metabolites in the *Bacillus subtilis* species complex. *mSystems* **6**, 10–1128 (2021).
50. Domínguez-Cuevas, P., Mercier, R., Leaver, M., Kawai, Y. & Errington, J. The rod to L-form transition of *Bacillus subtilis* is limited by a requirement for the protoplast to escape from the cell wall sacculus. *Mol. Microbiol.* **83**, 52–66 (2012).
51. Thomaides, H. B., Freeman, M., El Karoui, M. & Errington, J. Division site selection protein DivIVA of *Bacillus subtilis* has a second distinct function in chromosome segregation during sporulation. *Genes Dev.* **15**, 1662–1673 (2001).
52. Chastanet, A. & Carballido-López, The actin-like MreB proteins in *Bacillus subtilis*: a new turn. *Front. Biosc. (Scholar Ed.)* **4**, 1582–1606 (2012).
53. Billaudeau, C., Yao, Z., Cornilleau, C., Carballido-López, R. & Chastanet, A. MreB forms subdiffraction nanofilaments during active growth in *Bacillus subtilis*. *mBio* **10**, e01879–18 (2019).
54. Soufo, H. J. D. & Graumann, P. L. *Bacillus subtilis* actin-like protein MreB influences the positioning of the replication machinery and requires membrane proteins MreC/D and other actin-like proteins for proper localization. *BMC Cell Biol.* **6**, 10 (2005).
55. Bush, K. & Bradford, P. A. β-lactams and β-lactamase inhibitors: An overview. *Cold Spring Harb. Perspect. Med.* **6**, a025247 (2016).
56. Kaushik, D., Mohan, M., Borade, D. M. & Swami, O. C. Ampicillin: Rise fall & resurgence. *J. Clin. Diagnostic Res.* **8**, ME01 (2014).
57. Batson, S. et al. Inhibition of D-Ala: D-Ala ligase through a phosphorylated form of the antibiotic D-cycloserine. *Nat. Commun.* **8**, 1939 (2017).
58. Crisóstomo, M. I. et al. Attenuation of penicillin resistance in a peptidoglycan O-acetyl transferase mutant of *Streptococcus pneumoniae*. *Mol. Microbiol* **61**, 1497–1509 (2006).
59. Bedrunka, P. & Graumann, P. L. Subcellular clustering of a putative c-di-GMP-dependent exopolysaccharide machinery affecting macro colony architecture in Bacillus subtilis. *Environ. Microbiol. Rep.* **9**, 211–222 (2017).
60. Tsuge, K., Ano, T., Hirai, M., Nakamura, Y. & Shoda, M. The genes *degQ*, *pps*, and *lpa-8* (*sfp)* are responsible for conversion of *Bacillus subtilis* 168 to plipastatin production. *Antimicrob. Agents Chemother.* **43**, 2183–2192 (1999).
61. Gao, L. et al. Module and individual domain deletions of NRPS to produce plipastatin derivatives in *Bacillus subtilis*. *Microb. Cell Factories* **17**, 1–13 (2018).
62. Brantl, S. & Müller, P. Toxin-antitoxin systems in *Bacillus subtilis*. *Toxins* **11**, 262 (2019).
63. Park, J. H., Yamaguchi, Y. & Inouye, M. *Bacillus subtilis* MazF-bs (EndoA) is a UACAU-specific mRNA interferase. *FEBS Lett.* **585**, 2526–2532 (2011).
64. Martin, M. et al. De novo evolved interference competition promotes the spread of biofilm defectors. *Nat. Commun.* **8**, 15127 (2017).
65. Nawel, Z., Rima, O. & Amira, B. An overview on *Vibrio* temperate phages: Integration mechanisms, pathogenicity, and lysogeny regulation. *Microb. Pathog.* **165**, 105490 (2022).
66. Gavric, D. & Knezevic, P. Filamentous *Pseudomonas* phage Pf4 in the context of therapy-inducibility, infectivity, lysogenic conversion, and potential application. *Viruses* **14**, 1261 (2022).
67. Pasquina-Lemonche, L. et al. The architecture of the Gram-positive bacterial cell wall. *Nature* **582**, 294–297 (2020).
68. Mueller, E. A. & Levin, P. A. Bacterial cell wall quality control during environmental stress. *MBio*, **11**, 10-1128.
69. Errington, J. L-form bacteria, cell walls and the origins of life. *Open Biol.* **3**, 120143 (2013).
70. Dienes, L. & Weinberger, H. J. The L forms of bacteria. *Bacteriol. Rev.* **15**, 245–288 (1951).
71. Devine, K. M. Bacterial L-forms on tap: an improved methodology to generate *Bacillus subtilis* L-forms heralds a new era of research. *Mol. Microbiol.* **83**, 10–13 (2012).
72. Bryskier, A. *Antimicrobial Agents: Antibacterials and Antifungals*, 470-474 (Wiley Online Library, 2005).
73. Reusser, F. Effect of spectinomycin on peptide chain initiation. *J. Antibiot.* **29**, 1328–1333 (1976).
74. Parisien, A., Allain, B., Zhang, J., Mandeville, R. & Lan, C. Q. Novel alternatives to antibiotics: bacteriophages, bacterial cell wall

hydrolases, and antimicrobial peptides. *J. Appl. Microbiol.* **104**, 1–13 (2008).
75. Grabowski, Ł et al. Bacteriophage-encoded enzymes destroying bacterial cell membranes and walls, and their potential use as antimicrobial agents. *Microbiol. Res.* **248**, 126746 (2021).
76. Young, R. Y. Bacteriophage lysis: mechanism and regulation. *Microbiol. Rev.* **56**, 430–481 (1992).
77. Pohane, A. A. & Jain, V. Insights into the regulation of bacteriophage endolysin: Multiple means to the same end. *Microbiology* **161**, 2269–2276 (2015).
78. Vermassen, A. et al. Cell wall hydrolases in bacteria: insight on the diversity of cell wall amidases, glycosidases and peptidases toward peptidoglycan. *Front. Microbiol.* **10**, 331 (2019).
79. Derdouri, N., Ginet, N., Denis, Y., Ansaldi, M. & Battesti, A. The prophage-encoded transcriptional regulator AppY has pleiotropic effects on *E. coli* physiology. *PLoS Genet* **19**, e1010800 (2023).
80. Bucher, M. J. & Czyż, D. M. Phage against the Machine: The SIE-ence of Superinfection Exclusion. *Viruses* **16**, 1348 (2024).
81. Bernard, C., Li, Y., Lopez, P. & Bapteste, E. Beyond arbitrium: identification of a second communication system in *Bacillus phage* phi3T that may regulate host defense mechanisms. *ISME J.* **15**, 545–549 (2021).
82. Guler, P. et al. Arbitrium communication controls phage lysogeny through non-lethal modulation of a host toxin–antitoxin defence system. *Nat. Microbiol.* **9**, 150–160 (2024).
83. Loyo, C. L. & Grossman, A. D. A phage-encoded counter-defense inhibits an NAD-degrading anti-phage defense system. *PLoS Genet* **21**, e1011551 (2025).
84. Cardinale, C. J. et al. Termination factor Rho and its cofactors NusA and NusG silence foreign DNA in *E. coli*. *Science* **320**, 935–938 (2008).
85. Conter, A., Bouché, J.-P. & Dassain, M. Identification of a new inhibitor of essential division gene *ftsZ* as the *kil* gene of defective prophage Rac. *J. Bacteriol.* **178**, 5100–5104 (1996).
86. Govindarajan, S., Marepalli, A. & Nandhakumar, M. KilR of *E. coli* Rac prophage is a dual morphogenetic inhibitor of bacterial cell division and elongation machineries. *mSphere* **8**, e0102924 (2025).
87. Zhang, P. et al. Bacteriophage protein Gp46 is a cross-species inhibitor of nucleoid-associated HU proteins. *Proc. Natl Acad. Sci. USA* **119**, e2116278119 (2022).
88. Liu, J. et al. Virus-induced cell gigantism and asymmetric cell division in archaea. *Proc. Natl Acad. Sci. USA* **118**, e2022578118 (2021).
89. Burkholder, P. R. & Giles, N. H. Induced biochemical mutations in *Bacillus subtilis*. *Am. J. Bot.* **34**, 345–348 (1947).
90. Spizizen, J. Transformation of biochemically deficient strains of *Bacillus subtilis* by deoxyribonucleate. *Proc. Natl Acad. Sci. USA* **44**, 1072–1078 (1958).
91. Conn, H. J. The identity of *Bacillus subtilis*. *J. Infect. Dis.* **46**, 341–350 (1930).
92. Zeigler, D. R. et al. The origins of 168, W23, and other *Bacillus subtilis* legacy strains. *J. Bacteriol.* **190**, 6983–6995 (2008).
93. Schirner, K. & Errington, J. The cell wall regulator σI specifically suppresses the lethal phenotype of *mbl* mutants in *Bacillus subtilis*. *J. Bacteriol.* **191**, 1404–1413 (2009).
94. Scheinpflug, K. et al. Antimicrobial peptide cWFW kills by combining lipid phase separation with autolysis. *Sci. Rep.* **7**, 44332 (2017).
95. Kiesewalter, H. T. et al. Genomic and chemical diversity of *Bacillus subtilis* secondary metabolites against plant pathogenic fungi. *mSystems* **6**, 10–1128 (2021).
96. Kohm, K. et al. The *Bacillus* phage SPβ and its relatives: a temperate phage model system reveals new strains, species, prophage integration loci, conserved proteins and lysogeny management components. *Environ. Microbiol.* **24**, 2098–2118 (2022).

Acknowledgements

The authors thank the students Miray Özverin and Gregor Maska for help with sporulation assays, and obtaining and preliminarily characterizing lysogenic strains. We thank Henrik Stahl for sharing *mreB* mutant and valuable advice in preparation of MreB-GFP constructs. We also thank Anja Pavlin and Matej Butala for assistance in preparing additional molecular tools, Ines Mandić Mulec and Kasia Mickiewicz for advice during the project, and Iztok Dogša for microscopy support. AD, VAF, JJL, and VG were funded by the European Union (ERC, PHAGECONTROL, 101041421). Views and opinions expressed are however those of the author(s) only and do not necessarily reflect those of the European Union or the European Research Council Executive Agency. Neither the European Union nor the granting authority can be held responsible for them. AD was also supported by the Slovenian Agency for Research and Innovation (Grant number P4-0116). MB and HF were supported by DFG grant BR2915/13-1. TA was supported by an ARIS grant P4-0097.

Author contributions

A.D., A.T.K., M.B., and R.H. conceived the project; V.A.F., H.F., J.J.L., A.M., and P.K. performed experiments. VG and TA performed bioinformatics analysis. V.A.F. and A.D. wrote the manuscript and all authors contributed to the final version.

Competing interests

The authors declare no competing interests.

Additional information

Supplementary information The online version contains supplementary material available at https://doi.org/10.1038/s42003-025-08672-x.

Correspondence and requests for materials should be addressed to Anna Dragoš.

Peer review information *Communications Biology* thanks Fabian Commichau, Katarzyna Mickiewicz and the other, anonymous, reviewer(s) for their contribution to the peer review of this work. Primary Handling Editor: Tobias Goris. [A peer review file is available].